Development of a Pulsed Radar Reflectometer for Compact Helical System Plasmas

Rostislav Pavlichenko

THESIS

Submitted to the Department of Fusion Science
School of Mathematical and Physical Science
The Graduate University for Advanced Studies
for the Degree of

DOCTOR OF PHILOSOPHY
in physics

National Institute for Fusion Science
Graduate University for Advanced Studies

June 1998

Abstract

Density is one of the main parameters to characterize a plasma. Microwave reflectometry has been used for the electron density profile and fluctuation measurements in many plasma devices. The advantages of the reflectometry are:

1. obtaining information about local plasma electron density (not line averaged value like in the case of interferometry);

2. requiring only a small port for access to the plasma ;

In this thesis a very young type of microwave reflectometry is treated: *pulsed radar reflectometer*. We have developed the pulsed radar reflectometer for Compact Helical System (CHS). Major emphasis will be placed on technical aspects. It must be also stressed that this work is the first trial for *helical systems*.

In the conventional reflectometry a wave of the specific frequency is launched towards the plasma to be reflected from the layer in the immediate vicinity of the critical density. The phase difference of the launched wave and reflected wave contains the information on the position of the reflecting layer. In the case of pulsed radar reflectometry, short ($\sim$1ns) microwave pulses are launched into the plasma. The pulse is reflected from a corresponding critical density layer and received by the time of flight measurement system. The measured quantities for those types of reflectometers are phase or time delay. The advantages of the pulsed radar are as follows in comparison with the conventional reflectometry:

1. temporary losses of the reflected signal are not so serious, each pulse carries all information about the position of the critical density layer;

2. false reflection from window, horn lens or waveguides could be easily filtered, because they all occur outside of interested time window;

3. due to the very short time for the microwave propagation, plasma fluctuations seem to be "frozen" and they will not affect the measurements significantly;

4. effect of mode coupling becomes less critical because reflected ordinary and extraordinary mode pulses arrive at the different time; simultaneous measurements of O- and X-mode reflection are in principle possible yielding the total magnetic field;

Numerical simulation has been done to study the propagation and detection processes of the microwave pulses. Due to the dispersion in plasmas, the pulse shape of the microwaves is deformed. This deformation causes timing error in the Constant Fraction Discriminator (CFD), which yields a logic pulse. This discriminator is inevitable for our system to do amplitude insensitive measurements. The pulse deformation is more serious for shorter pulse width, and leads to a larger error in the timing. We have found that the errors decrease with the increase of the pulse width and errors are negligible (less than 1%) for pulse width longer than about 1 ns.

A 1-channel (with changeable frequency 51, 54, 57 GHz) pulsed radar system has been designed for CHS. It is similar to that developed by RTP tokamak group, where pulsed radars were introduced for the first time. The difference is

that our system uses bandpass filters at the IF stage, and can be upgraded to a multichannel system more easily. The system consists of:

1. microwave pulse production part;
2. microwave transmission, vacuum window and antenna, bandstop filter;
3. mixer and IF pulse electronics;
4. time of flight measurement electronics

To produce a suitable microwave pulse (short, large amplitude and well shaped) we tested special nonstandard fast switches (Millitech fast PIN switch and IRE varactor-diode fast modulator). The minimum pulse widths are 1.9 ns and 0.28 ns, respectively with heterodyne type detection, and the output power is around 50 mW at the peak of amplitude. Since a serious pulse broadening occurs in the long fundamental waveguide (WG), its length has been minimized. Although two independent launching and receiving antennas are used for most reflectometers, we use only one antenna for launching and receiving. This causes the problem that a small reflection ($\sim 2\%$) at the vacuum window makes a false pulse. In principle, the problem does not affect the measurements, because the false reflection occurs at a time window different from that for the true reflection (from plasma). This is the advantage of pulsed radar reflectometry. By using another PIN switch in front of the mixer we have succeeded for the first time in reducing the effect of false reflection to a practically acceptable level. Since the frequencies of ECH and reflectometer are rather close each other, we use a bandstop filter to reject strong ECH microwaves. Instead of an RF detectors, we

use a mixer and IF electronics, so that the system has a good signal to noise ratio (SNR), and the potential for the multichannel system. A CFD yields the peak timing of the reflected pulse, and the timing is independent of the amplitude. This is very useful for the measurements, because large amplitude change occurs often. A Time-to-Amplitude Converter (TAC) is used to measure the time delay of the reflected pulse. The output of the TAC is sampled by an Analog-to-Digital Converter (ADC).

Free space time measurements have been done to calibrate the timing electronics. Instead of the plasma cut-off layer, a metallic mirror is used and moved by 50-90 cm in front of the antenna. A spatial resolution of 0.3 cm has been reached, that comes from the accuracy of TAC output reading.

A 51GHz 1-channel pulsed radar reflectometer has been installed in CHS. As a wave polarization, ordinary and extraordinary modes are launched. We probed the plasma with microwave pulses of 1.9 ns. The plasmas were initiated by IBW (Ion Bernstein Wave) or ECH and heated by NBI and ECH. These measurements were done for discharges with the magnetic field of 0.85 T and the maximum electron density of about 6×10^{19} m^{-3}. At the first stage, we used an oscilloscope instead of CFD-TAC time of flight measurement electronics. Due to the function of oscilloscopes, we could get only one waveform for each discharge. The result showed that the reflected waveform was distorted but not significantly, and that in most cases the amplitude of the reflected pulses is rather small. When we read the peak timing by eyes, the relation between the time delay and the line averaged density agreed with the calculated curve both for O-/X-modes launching experiments.

As the next step, we used the CFD-TAC electronics by which we could get the time behavior for each discharge. The repetition rate of the pulse launching and measurement is 200 kHz. The launching polarity is adjusted to X-mode to measure relatively low density plasma. When the discharge starts, the density gradually increases. Below the critical density, the pulse passes through the plasma and is reflected at the back wall of the vacuum vessel. The reflected pulse passes through the plasma again and detected by the receiving system. This situation is called as delayometry. When the density increases, the cut off appears and moves towards the antenna. The time behavior of the time delay agrees with the calculation of this scenario by assuming the parabolic density profile. Instead of assuming the whole profile, we assume a linear profile between the plasma edge and the cut-off layer. Then the estimated position of the cut off layer coincides well with Thomson scattering measurements. The spatial accuracy of the determination of the position of the reflected layer during plasma measurements was about 5-8 mm.

While the reflectometer can follow the fast and large changes in density, the HCN interferometer fails, which is partly shown in the ice pellet injection experiment. The fast movement of the cutt-off density layer during the density collapse was successfully measured with the pulsed radar reflectometry. This fact demonstrates the reflectometer has a high temporal resolution.

The first pulsed radar measurements in a helical system have been done. We have succeeded in measuring the density with one antenna system, that means reflectometry requires only a small port. The density fluctuations could also be measured because of its high spatial and temporal resolution of pulsed radars.

Acknowledgements

I am especially grateful and indebted to my advisors Prof. Keisuke Matsuoka, Prof. Kazuo Kawahata and Dr. Akira Ejiri, for the guidance and encouragement they have shown me during my time here at National Institute for Fusion Science. Their friendly advice and intimidation never failed to guide me back on course when I seemed to be drifting.

I am most grateful and indebted to Director General of the National Institute for Fusion Science Prof. Atsuo Iiyoshi for his friendly advice and encouragement, which he has provided to me over the years.

Further help came from Prof. Shoichi Okamura and Mr. Chihiro Takahashi by introducing CHS data acquisition for me. I thank all other members of the CHS group for their insightful commentary on my work.

The rest of the inspiration for this work comes from Oleg S. Pavlichenko, my father. It was he who first suggested to me the idea of applying Pulse Radars to Stellarator configuration ...

Thanks, finally, to my dear wife Natali and son Oleg, who were always there with the large doses of love, patience, and encouragement.

The research was supported by the National Institute for Fusion Science and by a Fellowship from the Government of Japan (Monbusho).

Rostislav Pavlichenko

National Institute for Fusion Science

June 13, 1998

List of Figures

List of Tables

Contents

Chapter 1

Introduction

"The last thing that we find in making a book is to know what we must put first."

Blaise Pascal. 1623-1662.

Thermonuclear fusion with its almost inexhaustible resources has the potential of satisfying the ever-increasing need for energy in the world. In the attempt to achieve controlled thermonuclear fusion, 'helical systems' (stellarators) are considered being serious contenders to tokamaks. The plasma confinement in helical systems requires reliable control and diagnostic tools. This chapter will describe thermonuclear fusion basics and will give a short tour on Compact Helical System stellarator, although it will provide main aim of this thesis.

1.1 Plasma and nuclear fusion

In recent years there has arisen considerable interest in the plasma state of matter. The rapidly expanding research areas include thermonuclear fusion, high-energy particle acceleration, magnetospheric physics and cosmic ray physics. *Fusion* is the process that energizes the sun and stars. Future energy needs will require contributions from many sources, and fusion might become one of the most attractive sources. Basically, plasma is a collection of charged particles that interact with each other by means of the 'long-range' Coulomb force. These give rise to collective modes not found in neutral gases. One characteristic plasma scale length is the Debye length

$$\lambda_D = \{KT/\left(4\pi n_0 e^2\right)\}^{1/2}$$

where K is the Boltzmann's constant, T is the electron temperature, n_0 is the electron density, and e is the electron charge. There are also two characteristic frequencies, the *plasma frequency* and *cyclotron frequency*, that prove to be useful in our description of plasma. The plasma frequency $\omega_{pe} = \sqrt{4\pi n_0 e^2/m_e}$ and is the frequency at which particles displaced from their equilibrium positions will oscillate due to the electrostatic Coulomb restoring force. For electrons $f_{pe} = \omega_{pe}/(2\pi) = 8.98 \times 10^3 \sqrt{n_e\,(cm^{-3})}$. The cyclotron frequency $\omega_c = qB/\left(m_q c\right)$ is the frequency at which charged particles gyrate about the magnetic field lines of strength $|\vec{B}|$. For electrons $f_{ce} = \omega_{ce}/\left(2\pi\right) = 27.99 \times B\,(T)\,[GHz]$.

Much effort aimed at understanding the plasma state has been oriented toward the achievement of controlled thermonuclear fusion. Controlled thermonuclear fusion utilizes hydrogen and its two isotopes, deuterium and tritium, for its

fuel.

The first-generation fusion reactors will use deuterium and tritium for the fuel because they will fuse at lower temperature. In the fusion reaction deuterium and tritium nuclei combine together, or fuse, to form helium nucleus and energetic neutron. During the fusion reaction, a small amount of mass appears to be lost, but the matter has been converted to energy following `Einstein's` famous equation $E = mc^2$. Even a very small mass can yield a considerable amount of energy.

$$
\begin{aligned}
{}^1\mathrm{D}_2 + {}^1\mathrm{T}_3 &= {}^2\mathrm{He}_4\ (3.52\ \mathrm{MeV}) + {}^0\mathrm{n}_1\ (14.06\ \mathrm{MeV}) \\
{}^1\mathrm{D}_2 + {}^1\mathrm{D}_2 &= {}^2\mathrm{He}_3\ (0.82\ \mathrm{MeV}) + {}^0\mathrm{n}_1\ (2.45\ \mathrm{MeV})\ (50\ \%) \\
{}^1D_2 + {}^1D_2 &= {}^1T_3\ (1.01MeV) + {}^1p_1\ (3.02MeV)\ (50\%) \\
{}^1D_2 + {}^2He_3 &= {}^2He_4\ (3.67MeV) + {}^1p_1\ (14.7MeV)
\end{aligned}
$$

Three methods for plasma confinement are currently known – gravitational confinement which is used in stars but is not possible on the earth, inertial confinement, and magnetic confinement. Inertial confinement uses pulsed energy sources (e.g. laser beam) to concentrate energy on a small frozen pellet of fusion fuel. This pulsed energy source compresses the pellet up to a thousand times of the normal solid density and heats the fuel to ignition temperature. Magnetic confinement uses magnetic fields to hold plasma (ionized gas) in place while it is heated to ignition temperature by external sources. There are several types of devices to produce and confine the plasma. The most promising devices among them are tokamak and helical system.

1.2 Helical Systems

The helical systems are generally considered to be the most hopeful alternative to the tokamak. Since the concept is inherently of steady state, it would not have the tokamak's problems; thermal and mechanical cycling, current drive, and disruptions. To achieve these promising performance features, stellarator sacrifices the toroidal symmetry of tokamaks and is fully three-dimensional toroidal plasma devices.

Device named *stellarator* was invented in 1951 by `Lyman Spitzer` [1]. Today helical systems have a vide variety in the configurations. They could be divided into two main groups depending on the type of the magnetic axis formation method.

- Planar axis configuration: classical stellarator, heliotron/torsatron;
- Spatial axis configuration: figure-8 like, modular coil system, Heliac, Helias.

In the helical devices with planar axis, the confining magnetic field is produced by a combination of the helical, vertical and toroidal field coils. The closed magnetic surfaces, could have different cross section shape. It depends on the poloidal coils number[1] l. The vertical field coils are necessary to cancel vertical part of the field produced by the helical coils. This approach was realized in `Heliotron E` toroidal device. However, the toroidal field coils are not necessary to produce the confining field, but can be used to change such the field properties as rotational transform, shear and volume of the confining region. It should be

[1] ...closed magnetic surfaces have elliptical l=2, triangular – l=3 , or rectangular – l=4 shape...

noted than only the helical and vertical coils are required to produce a closed magnetic surfaces (approach that realized in `ATF, CHS, LHD machines`).

Helical systems with spatial axis are the competitive modification of the helical device. This idea was realized the in `Wendelstein 7-AS` stellarator. The magnetic surfaces could be created by the set of non-planar, non-circular coils. In this device there is some flexibility for changing the configuration with respect of rotational transform, magnetic ripple and plasma position, by using the independent power supplies in the additional planar coils, the modular corner coils and the vertical field coils respectively.

The largest magnetic fusion machines that were just built or under construction are two superconducting stellarators: Large Helical Device (LHD) in Japan[2] [2] and the Wendelstein 7-X (W7-X) in Germany[3] [3]. The plasma parameters achieved in present stellarator experiments are second to those in tokamaks: the energy confinement time is as long as 43 msec [4], the ion temperature as high as 1.6 keV [5], the electron temperature as high as 6 keV [6], the plasma density as high as $2 \times 10^{20} m^{-3}$ [5], and the volume-averaged plasma beta (β – plasma pressure over magnetic pressure) up to 2.1% [7].

[2]...at National Institute for Fusion Science; which started operation on March 31, 1998

[3]...at Max–Planck–Institut für Plasmaphysik; which is to start operation in 2004

1.3 Compact Helical System (CHS)

1.3.1 Magnetic configuration in CHS

The Compact Helical System (CHS)in the National Institute for Fusion Science is one of the *heliotron/torsatron* type devices [8]. It is characterized by its low aspect ratio. The main device parameters are as follows; major radius $R_0 = 100cm$, plasma minor radius $\overline{a_{pl}} = 20cm$, toroidal magnetic field $B_t = 2T$, $l = 2$, $m = 8$ (the full set of the CHS parameters is given in Table 1.1). The rotational transform ι in the vacuum condition monotonically increases from 0.3 at the magnetic axis to around 1.0 at the last closed flux surface. Three of poloidal coils which can be controlled individually (coil current and its direction) enable the magnetic configuration (the rotational transform, the magnetic well, shear and field ripple profiles) to vary over a wide range. This flexibility, which consists in magnetic axis shift and elongation of the plasma minor cross-section, is the key tool for studying the helical plasma confinement.

The target plasma is typically produced by the electron cyclotron heating (ECH) of mainly 53.2 GHz and the power up to 500 kW. The ion cyclotron resonance heating (ICRH) system of 7.5 MHz is also available for the plasma production. Two neutral beam injectors (NBI) are installed on CHS to sustain and heat the target plasma. NBI #1 is typically operated with the injection energy of 40 kV and the port through power of 1.1 MW. The injection angle can be varied from tangential to perpendicular. NBI #2 is operated with the injection energy of 36 kV and the port through power of 0.7 MW. As another auxiliary heating equipment, five antennas of the ion cyclotron range of frequency (ICRF)

Parameter	Value	Units
DEVICE PARAMETERS		
major radius of the vacuum vessel, R_0	100	cm
helical coil radius, a_c	31.3	cm
averaged minor plasma radius, $\overline{a_{pl}}$	20	cm
aspect ratio, $A_p = R_0/\overline{a_{pl}}$	5	
toroidal magnetic field at the helical winding center, $B_t(0)$	0.7 – 2.0	T
multipolarity, l	2	
toroidal period number, m	8	
pitch parameter, γ_c	1.25	
pitch modulation, α^*	0.3	
rotational transform angle (axis), ι_{axis}	0.3	
rotational transform angle (edge), ι_{edge}	0.9 – 1.1	
plasma current, I_{pl}	0	
HEATING SYSTEMS		
NBI #1 (co-injection, in standard operation)	1.10	MW
NBI #2 (counter-injection, in standard operation)	0.70	MW
ECH #1, 53.2 GHz	0.50	MW
ECH #2, 106.4 GHz	0.50	MW
ICRF (IBW), 7.5 GHz	0.25	MW

Table 1.1: *Main parameters of the CHS device and heating systems*

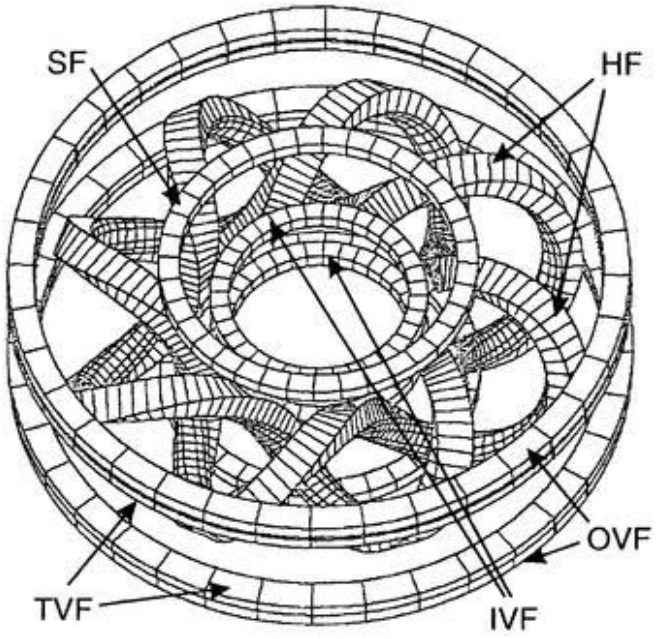

Figure 1.1: *The schematic plot of the CHS magnetic coils, HF – Helical Field Coil, SF – Shaping Field Coil, OVF – Outer Vertical Field Coil, IVF – Inner Vertical Field Coil , TVF – Trimming Vertical Field Coil*

of 26 MHz were installed in the outboard high field side. Via above mentioned antennas the power of 1.5 MW could be transferred to the plasma.

During last years in CHS the following experimental subjects have been primarily studied:

- MHD equilibrium and stability;
- energy and particle transports;
- high-energy-particle confinement;

1.3.2 Overview of CHS main diagnostics

In order to measure the plasma parameters in CHS, many different diagnostic systems have been developed and installed. With these diagnostics either electromagnetic radiation or particle released from the plasma are measured, in other words, the plasma is probed without disturbing the main parameters. Here we briefly describe the main CHS diagnostic. In general we can divide all diagnostics into two main classes: *monitoring diagnostics* and *profile diagnostics.* Main CHS diagnostics are plotted in Figure 1.2.

The HCN laser interferometer system

The HCN laser interferometer system, used to measure the line averaged plasma electron density, utilizes the wavelength of 337 μm. The laser beam is directed along different paths, some through the plasma and one through the reference path outside the plasma. The electron density changes the optical path length

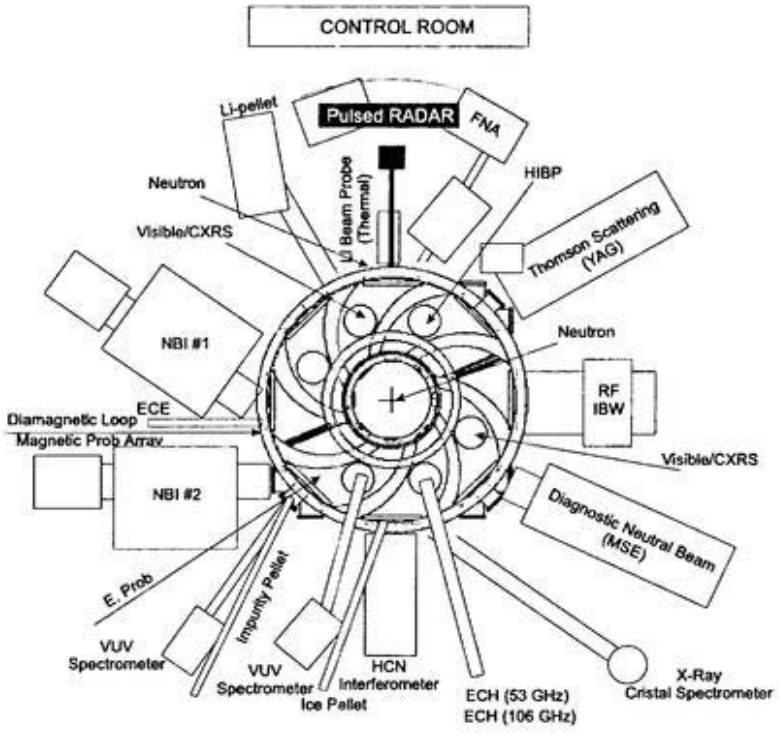

Figure 1.2: *The schematic plot of the main CHS diagnostics*

of the waves in the plasma and this change is compared with the reference path length. The HCN laser interferometer has three horizontal chords, with non-equidistant spacing over the plasma diameter. The information obtained corresponds to the line-integrated density; this information is used to determine the density profile by an Abel inversion routine. In the inversion procedure the calculated position of the magnetic flux surfaces in CHS is used; it is assumed that the electron density is constant on those surfaces. Profiles are obtained with the typical measuring time of 10 μsec.

The YAG Thomson scattering measurement system

The YAG Thomson scattering measurements are based on the fact that electromagnetic radiation at the employed wavelength of 1.6 μm is scattered by free electrons in the plasma. The scattered waves are shifted in frequency due to thermal velocities of electrons. In CHS five Nd:YAG lasers with high power are pulsed at 50 Hz repetition rate to produce a 10 cm long wave package which is launched along the midplane, from the outboard side of the torus. The intensity of back-scattered radiation received is proportional to the electron density. The electron temperature can be determined from the frequency shift of the radiation.

The heavy ion beam probe (HIBP)

A 200 keV heavy ion beam probe (HIBP) [10, 11] is a useful diagnostic instrument to measure the local plasma potential and its fluctuations with fast time response in magnetically confined plasmas. In potential measurements a singly charged HIB (primary beam) is injected in the target plasma and then a doubly charged

ion created due to of an electron impact ionization (secondary beam) comes out with the energy change corresponding to the plasma potential at the ionizing point. For full radial potential profile measurements it takes 4 msec to scan the plasma. Radial electric field profiles of the CHS plasmas are obtained from the measured space potential profiles. Also by use of this diagnostic potential fluctuations (up to 100kHz) in hot (>100 eV) plasma could be measured.

The fast neutral particle analyzer (FNA)

Because of low aspect ratio of the CHS device the orbit loss of high energy particles (due to non-axisymmetric magnetic field ripple structure) could be significant. This loss of high energy particles should make large contribution to the global energy confinement of the high temperature plasma in helical systems. The fast neutral particle analyzer (FNA) [14, 15] is developed to measure the energy spectrum of the high-energy ions. Also this diagnostic is very useful to get an important information on the heating efficiency during various heating experiments in CHS. The FNA has 20 micro-channel plates for ion energy up to 50 keV. The supporting structure of the FNA could be moved to both vertical and horizontal directions. 2-D ion distribution in the velocity space ($\vec{v}_{\parallel}$ and $\vec{v}_{\perp}$ with the respect to the magnetic field) could be obtained by the horizontal scan for different pitch angle ions. By vertical scan it is possible to measure the energy spectrum of ions from different parts of the plasma.

The charge exchange recombination spectroscopy (TVCXS)

For the evaluation of plasma energy transport the ion temperature must be known as well as the electron one. The radial profiles of ion temperature for various plasma scenarios in CHS are measured with the television charge-exchange spectroscopy (TVCXS) by the use of the neutral beam heating in CHS [12, 13]. Ion temperature profiles have been obtained with the C^{VI} charge-exchange recombination (CXR) line using a space- and wavelength-resolving visible spectrometer installed on the CHS. Two sets of 30-channel optical-fiber arrays, one viewing a fast neutral hydrogen beam (CXR channels) and the other viewing off the neutral beamline (background channels), are arranged on the entrance slit of the spectrometer. This spectrometer is coupled to an image intensifier and CCD detector at the focal plane, and provides the temperature profile every 20 msec. The ion temperature is derived from the Doppler-broadened line profile after subtracting the simultaneously measured cold component (background channels), which is due to electron excitation and/or charge-exchange recombination in the plasma periphery.

1.3.3 Various heating scenarios and typical discharges

During past years of operation CHS has been equipped with various heating systems. Neutral beam system installed on CHS has two beam lines, NBI#1 and NBI#2. The injection angle of NBI#1 can be changed from nearly perpendicular to parallel. ECH system consists of two gyrotrons. One of the gyrotrons oscillates at 53.2 GHz with the power of 400 kW and the other at 106.1 GHz with 450 kW.

This allows performing different plasma experiment scenarios.

The operation conditions in CHS could be divided into several parts:

- 'standard operation';
- high β plasma;
- high T_i-mode;

Standard operation mode is realized for various plasma experiments. It is characterized by low magnetic field (typically 0.8–0.9 T), any plasma axis position[4], with ECH(IBW) plasma production and NBI#1 (co-injection) heating. The central electron density varies from 3 to $4 \times 10^{19} m^{-3}$. To control the plasma density (n_e) both gas puffing and Ti-gettering could be used.

High β plasma regime is characterized by inward shifted (0.921 m–0.949 m) plasma (because of additional β related plasma shift). Plasma is produced by IBW and heated with consequent injection of both neutral beams (second NI starts injection after sufficient increase of the electron density). For further increase of the plasma density gas puffing is implemented as well as strong wall conditioning.

The high ion temperature mode (High-T_i-mode) operation scenario aims on getting of high performance plasma without gas puffing. Such kind of regime utilizes heating power from both 53.2 GHz gyrotrons with combination of NB. Because of high performance high-magnetic field operation (up to 1.8 T) is chosen. High-T_i-mode in the low density [5] regime, and inward shifted plasma

[4] the plasma axis position could be changed from 0.874 m to 1.02 m

[5] with typical central electron density $1.0 - 1.5 \times 10^{19} m^{-3}$

position is characterized by high ion temperature in the core plasma and peaked electron density profile.

1.4 Purpose of this thesis

Recently growing attention to the reflectometry [18, 19, 21, 20], as the suitable diagnostic for plasma density profile and density fluctuations measurements, has been given. In the past several years, reflectometry introduced several new promising approaches such as amplitude modulation, ultrafast frequency sweeping and others [22, 23, 24] . One of them was pulsed radar [25, 26, 27]. It has been shown that in tokamak plasma experiments the pulsed radar works reliably giving density profiles which are comparable to those from other diagnostics (Thomson scattering and interferometry).

At the proposal phase of project we took into account the available information on the range of plasma densities of interest on CHS, required space and time resolution of profile measurement, possible porting of launch/receive antennas and available funding for project.

For the first trial we have chosen a frequency range in the vicinity of 50 GHz that allows probing plasma layers with the electron density in the range of $10^{19}m^{-3}$. (See Figure 1.3). As existing diagnostics on CHS have a radial resolution of profile measurements in the range of 0.02 m (Thomson scattering) and this resolution is not enough for measurement of steep gradient edge plasma, we aimed on achievement of radial resolution in the range of 0.005 m. This goal required the use of microwave pulses with the width of well below 1 ns.

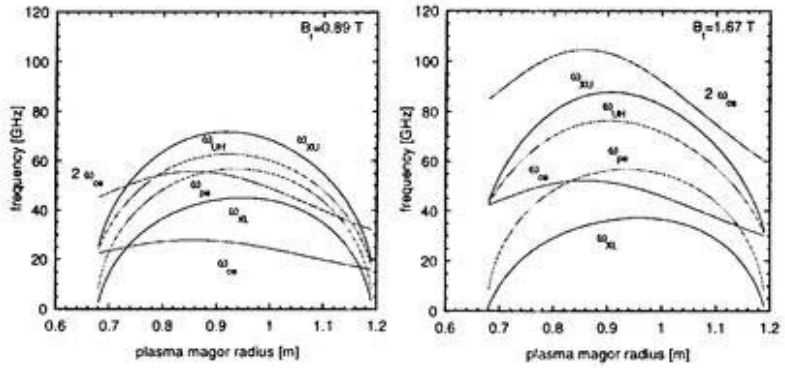

Figure 1.3: *The characteristic frequencies for the main regimes of CHS operation (a) low field case (B_t=0.89 T); (b) high density case (B_t=1.67 T), where ω_{pe} – electron plasma frequency, ω_{ce} – electron cyclotron frequency, $2\omega_{ce}$ – electron cyclotron frequency second harmonic, ω_{pe} – electron plasma frequency (O-mode), ω_{UH} – upper-hybrid frequency, ω_{XU} – upper cut-off (X-mode), ω_{XL} – lower cut-off (X-mode)*

The pulsed radar project has started on CHS when the most diagnostic ports were already used by a numerous important diagnostics. Therefore the room for single antenna porting on outer diagnostic port (#7O) was allowed in the first phase of project. This port allows to launch a microwave beam along the large axis of elliptically shaped CHS plasma column. As it will be seen from results this probing direction imposed an additional severe problem of reflected signal power diminution due to microwave beam refraction when it is reflected from the plasma layer with the stronger curvature than that in cylindrical tokamak with the same average plasma radius. But this problem is inevitable for l=2 Heliotron/torsatrons (CHS, LHD) and should be overcome to prove the applicability of pulsed radar for these devices. Having in mind previous experience on tokamaks we suggested that microwave oscillators with the output power of 50-100 mW and the heterodyne receivers of reflected signal will be used as well as a time-of-flight techniques similar to previous experiments.

All previous systems of pulsed radar used the separate launching and receiving antennas. The possibility to port only the single launching/receiving antenna for pulsed radar imposed the problem of reflection of launching pulse from vacuum window of channel. The successful solution of this problem could give the information valuable for implementation of pulsed radar on ITER where the use of the single launch/receive antennas for pulsed radar diagnostic was strongly recommended as one of topics of R&D on the ITER CDA phase.

Chapter 2

Reflectometry

In magnetically confined plasmas, the application of the radio frequency waves (interferometry, reflectometry, radiometry) is considered to be one of the most promising methods for plasma diagnostics. To date, microwave reflectometry has been widely used to measure the density profile and the density fluctuations in various fusion experimental devices. All the methods in the modern reflectometry determine the time delay through the phase difference measurement. In order to overcome the fluctuations problem, an alternate solution (pulsed radar) is to launch a short pulse at a given frequency and directly measure the time of flight of the reflected echo.

2.1 Introduction to reflectometry

Since 1959, research programs in controlled nuclear fusion, have induced a great progress in the study of plasma properties. To understand a number of fundamental processes occuring in the plasma, the knowledge of the electron density spatial distribution is of major interest.

For laboratory plasmas, electron density has been measured by a microwave technique which uses the reflection of the wave from the layer where the incident frequency $f = \omega/2\pi$ is equal to the plasma frequency $f_{pe} = \omega_{pe}/2\pi$. In other words reflectometry is based on the total reflection experienced by microwave from the plasma layer where the *refractive index* $\mu(\vec{r}, \vec{B}_t)$ vanishes. This phenomenon has been known as the *microwave cutoff*.

In magnetized plasmal there are two posibilities of the wave polarization. In principle, both of *ordinary mode* $\vec{E} \parallel \vec{B}_0$ (with its electric field parallel to the external magnetic field) and *extraordinary mode* $\vec{E} \perp \vec{B}_0$ (with its electric field perpendicular to the external magnetic field) may be used for reflectometry applications. The plasma refractive indexes for the ordinary and extraordinary modes are given by the formulas:

$$\mu_o^2 = 1 - \frac{f_p^2}{f^2} \tag{2.1}$$

(2.2)

$$\mu_x^2 = 1 - \frac{f_p^2}{f^2}\left(\frac{f^2 - f_p^2}{f^2 - f_p^2 - f_{ce}^2}\right) \tag{2.3}$$

Here f_p, f_{ce} are corresponding plasma and electron cyclotron frequencies.

$$f_p = \frac{1}{2\pi}\left(\frac{4\pi e^2 n_e}{m_e}\right)^{\frac{1}{2}} \tag{2.4}$$

$$f_{ce} = \frac{1}{2\pi}\left(\frac{eB}{m_e c}\right) \tag{2.5}$$

In the reflectometry the relative movement of the cut-off layer could be obtained either form the change in the phase difference between the reference and the reflected waves (conventional reflectometry) or from deducing the delay time between incident and reflected microwave pulses (pulsed radar reflectometry). As the pulsed radar technique is the main subject of this thesis we will discuss it in the separate section. Here we want only to introduce the basis of conventional reflectometry.

It was mentioned above that the quantity that is measured by reflectometer is phase of the microwaves reflected from the plasma (with comparison with the phase of the 'reference' signal). To obtain phase difference theoretically (in one dimensional approximation) one must solve the wave equation,

$$\frac{d^2E}{dr^2} + \mu^2 k_0^2 E = 0 \tag{2.6}$$

WKB solution[1] is well known for this equation, where the changes in the refractive index are small compared to the wavelength ($\mid \nabla k \mid /k^2) \ll 1$

$$E(r,t) = E_0 \exp\left(i\omega_0 t + i(k_0 \int_r \mu dr + \frac{\pi}{4})\right) \tag{2.7}$$

where $\omega_0 = 2\pi f_0$ is the angular frequency of the incident wave. The corresponding phase [16, 17] could be presented by

$$\varphi(\omega_0) = 2k_0 \int_{r_{ant}}^{r_{coff}} \mu(r)dr + \frac{\pi}{2} = \frac{2\omega_0}{c} \int_{r_{ant}}^{r_{coff}} \mu(r)dr + \frac{\pi}{2} \tag{2.8}$$

[1]...approximate solution to wave equation for inhomogeneous media is usually called Wentzel-Kramer-Brillouin (WKB) approximation, it holds when inhomogeneities are small ...

Here k_0 is the incident wavenumber, r_{ant} is the antenna position, r_{coff} is the position of the cut-off layer. For O-mode reflectometry, the phase change due to the plasma is given by [16, 17]:

$$\varphi(\omega_0) = \frac{2\omega_0}{c} \int_{r_{ant}}^{r_{coff}} \sqrt{1 - \frac{\omega_p^2}{\omega_0^2}}\, dr + \frac{\pi}{2} \tag{2.9}$$

The integral in Eq. 2.9 does not take into account the breakdown of the 'geometrical optics' (the WKB-approximation) near the reflection point. However, one-dimensional full-wave calculations show that it is usually allowed [37]. The 'extra factor' $\pi/2$ shows the additional phase 'jump' due to the reflection. To obtain the position of the reflection that occurs in the plasma, the probing frequency is needed to be swept (gradually changed). The phase change with respect to the frequency sweeping gives a time of flight of the microwave signal during the propagation through the plasma [16, 17]:

$$\tau_{pe}(\omega_0) = \left(\frac{\delta\varphi(\omega)}{\delta\omega}\right)_{\omega=\omega_0} = \frac{2}{c} \int_{r_{ant}}^{r_c(\omega_0)} \frac{1}{\sqrt{1 - \frac{\omega_p^2}{\omega_0^2}}}\, dr \tag{2.10}$$

2.2 Detection technique in the reflectometry

Recently many different reflectometer systems have been developed. They utilize different techniques to measure plasma phase shift. Some of them will be discussed here. We have no intention to give the full overview of this field of plasma diagnostic, but we only want to mention the most common one of them.

2.2.1 Homodyne detection

The homodyne detection technique is the oldest and the simplest one. The basic

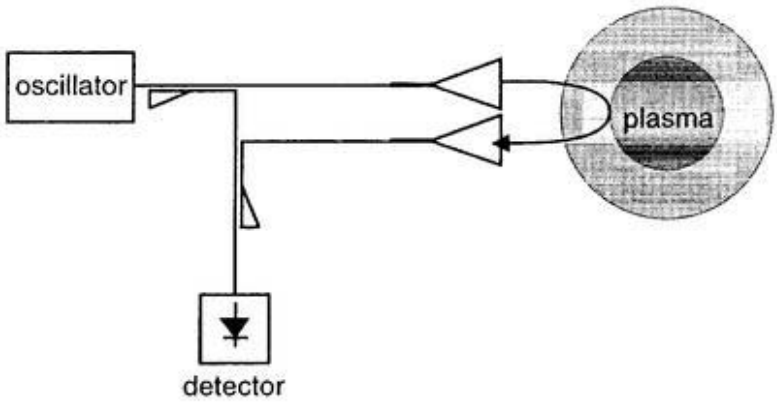

Figure 2.1: *The schematic plot of the single homodyne reflectometer*

detection scheme is shown in Figure 2.1. This system utilizes only single detector. The signal reflected from the plasma ($e_1(t) = A(t)\cos(\omega t + \varphi(t))$) and the signal going through the 'reference' arm of the reflectometer ($e_2(t) = B\cos(\omega t)$, here $\varphi(t)$ - the phase change due to the path through the plasma) are combined at this squared-law detector. The output signal at the detector becomes,

$$D^{homodyne}(t) = \frac{1}{2}Q\left(A^2(t) + B^2 + 2A(t)B\cos(\varphi(t))\right) \tag{2.11}$$

In this expression Q represents the detector sensitivity. It is common practice to use the detectors with low-pass characteristics, so all high frequency components of the 'mixed' signal are filtered out. It is well known that this 'mixed' signal depends on both phase and amplitude of the signal reflected from the plasma. The disadvantages of this technique are that only in the case where $\varphi(t)$ exceeds π the

absolute level of the reflected power could be determined[2]. And it is impossible to evaluate the direction of plasma reflected layer movement.

To perform the absolute phase difference measurements the so-called 'quadrature-phase detection' technique was invented. In this case (see Figure

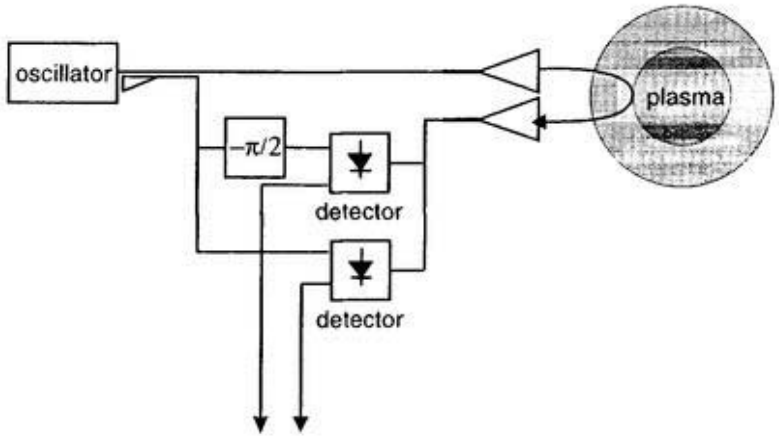

Figure 2.2: *The schematic plot of the quadrature-phase detection reflectometer*

2.2), the signal in the reference arm is split equally into two parts. Both parts are fed into equal detectors, and: before one of them additional phase shifter (with phase shift of π / 2) is inserted. In this case the outputs from the detectors

[2]... let's imagine that in 'stationary' case (there is no movement of the plasma reflected layer, so plasma density profile has a constant shape) the phase difference between reflected and reference signal becomes $2\pi \times n$, where n – number of wavelengths. Then $\cos(\varphi(t)) = 1$. After the start of the plasma movement the phase difference will occur between those two signals. The output of the detector will decrease no matter in what direction plasma will move ...

will be,

$$D_{cos}^{homodyne}(t) = \frac{1}{2}Q\left(A^2(t) + B^2 + 2A(t)B\cos(\varphi(t))\right) \quad (2.12)$$

$$D_{sin}^{homodyne}(t) = \frac{1}{2}Q\left(A^2(t) + B^2 + 2A(t)B\sin(\varphi(t))\right) \quad (2.13)$$

so 'sine' and 'cosine' parts of the signal can be measured independently. By removing the DC components and fulfilling the condition of $A(t) \ll B$, Equations 2.12, 2.13 can be rewritten to:

$$D_{cos}^{homodyne}(t) = QA(t)B\cos(\varphi(t)) \quad (2.14)$$

$$D_{sin}^{homodyne}(t) = QA(t)B\sin(\varphi(t)) \quad (2.15)$$

The power dependence characteristics of the detectors must be exactly the same to perform reliable measurements with this scheme. Also small dynamic range of the system (it comes from $1/f$ noise dependence of the detectors) could be a limitation in plasma measurements for big tokamaks and stellarators.

2.2.2 Heterodyne detection

To overcome the above mentioned limitation in detecting the reflected microwaves from the plasma, 'heterodyne detection technique' was introduced. For this case two oscillators must be used. One is used as a transmitter and the other is inserted in the reference arm. Those oscillators must be kept at constant frequency difference. This could be made by a phase lock loop (PLL). The RF signal (signal from launched oscillator that is reflected from the plasma) is fed through

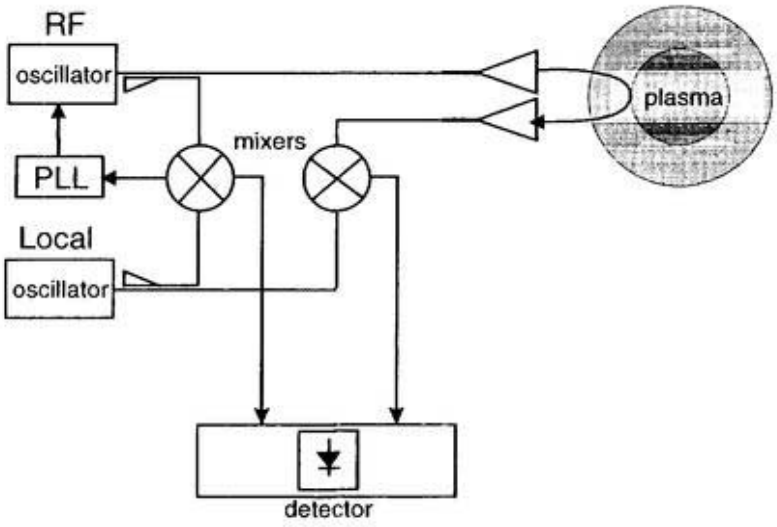

Figure 2.3: *The schematic plot of the heterodyne detection reflectometer; RF – source oscillator, LO – local oscillator, PLL – phase lock loop*

the waveguide system to the RF input of the mixer, while the LO signal comes directly from local oscillator. IF power detection is made by the IF detector. This power depends linearly on input power from the plasma (power from the RF port). The advantages of the heterodyne detection are in very high dynamic range.

2.3 Density profile measurements via reflectometry

Full wave calculations show that the total phase delay of an O-mode during propagation in the plasma and reflection at the cut-off layer is governed by Equation 2.8. In the O-mode case the density profile is determined by solving the Equation 2.8 by using Abel inversion technique,

$$R_{cut-off} = \frac{c}{\pi}\int_0^{f_c} \frac{1}{2\pi}\frac{d\varphi}{df}\frac{df}{\sqrt{f_c^2 - f^2}} \tag{2.16}$$

In the case of X-mode, the situation becomes more difficult. There is no analytical solution. The reason is that the plasma refractive index depends on the magnetic field (Eq.2.3) and on the plasma density as well. The profile reconstruction technique for X-mode was described in references [30, 52, 53].

As a general remark we want to add that reflectometers measure the phase difference of the carrier frequency. The main drawback is that the absolute phase difference becomes undetermined. So, it is impossible (without calibration of the reflected signal from some well known points in space) to obtain the absolute values of the plasma reflecting layer position. Some reference point that

could be given by means of other diagnostics is needed. Also it is very common situation that losses of the signal occur and it is no longer possible to reconstruct the density profile. For more reliable measurements some advanced methods were established, recently.

2.3.1 FM reflectometry

In order to determine the position of the reflecting layer, it is necessary to measure $(d\varphi/df)$ for the range of frequencies between 0 and f_p. But in the real experiment it is not possible to provide measurements down to zero frequency and the missing data must be provided from other diagnostics (probes, for instance). There are two main approaches to scan major part of density profile. In one case the frequency is swept over the broad range and $(d\varphi/df)$ is measured as a function of the frequency [24, 47, 46, 56]. Also it could be done by multi-frequency narrow-band sweeping reflectometry [41, 40], where the density profile is probed with 12-channel reflectometer. All channels are swept over 1% of the carrier frequency. The main important improvement that was done in recent years was introducing the ultra-fast frequency sweeping system that can sweep in $\geq 10\mu sec$ (previously the sweeping time was about 5-10ms). Linearity is not important because the $(d\varphi/df)$ curve is measured accurately with an automatic calibration procedure and is included in the data evaluation algorithm. As the plasma is nearly frozen during the probing interval, the effect of temporal fluctuations is greatly reduced. Amplitude and phase modulations originated by spatial turbulences are still observed and cannot be eliminated by sweeping faster, but this does not prevent the measurements even with high turbulence. A complete

profile is obtained from a single-frequency sweeping, without any sophisticated filtering or averaging procedure. Average profiles can also be obtained either from smoothing each $(d\varphi(f)/df)$ curve or averaging over some selected number of $(d\varphi/df)$ curves.

2.3.2 AM reflectometry

The ambiguity in phase measurements in the conventional reflectometry could be overcome by significant decrease of the phase change. In AM reflectometry the amplitude of the carrier wave is modulated by a long wave (about 100 MHz). The carrier frequency is reflected from plasma and the phase of the modulated signal φ_{Mod} is measured. Because of very long waves of the modulating signal it is possible to keep phase difference less than 2π. It must be noted that the velocity of the wave propagation is group velocity, not the phase velocity that is commonly used in conventional reflectometry. From this measurement the time delay in plasma could be obtained,

$$\varphi_M = \tau_p f_M = \frac{f_M}{c} \int^{r_c(f_0)} \frac{d(f_0 \mu(r))}{df_0} dr \tag{2.17}$$

and the density profile could be measured by using the multifrequency or single frequency sweep setup. However, the disadvantage of this method is that the wave envelope can be easily deformed by the false reflections from waveguides and windows. So it can reliably operate in two-antenna implementation only.

2.3.3 Pulsed radar

Recently a new approach for plasma density profile reconstruction was introduced [25, 26, 27]. In the case of pulsed radar reflectometry, short (~1ns) microwave pulses are launched into the plasma. The pulse is reflected by a corresponding critical density layer and received by the time measurement system. The measured quantities for those types of reflectometers are phase or time delay. Those experiments show that this rather young approach of the reflectometry becomes a promising tool for plasma profile evaluation. Previously pulsed radars were successfully operated on several tokamaks (RTP (Netherlands), START (UK), T-10 (Russia) and TEXTOR-94 (Germany)).

Here we present the first trial to port this diagnostic to the helical system. The advantages of the pulsed radar are as follows in comparison with the conventional reflectometry:

1. temporary losses of the reflected signal are not so serious, each pulse carries all information about the position of critical density layer

2. false reflection from window, horn lens or waveguides could be easily filtered, because they all occurred outside of interested time window;

3. due to the very short time for the microwave propagation, plasma fluctuations seem to be "frozen" and they will not affect the measurements significantly;

4. effect of mode coupling becomes less critical because reflected ordinary and extraordinary mode pulses arrive in different times; simultaneous measure-

ments of O- and X-mode reflection are in principle possible yielding the total magnetic field;

As this diagnostic forms the main subject of this thesis it will be discussed in the separate part.

2.3.4 Ultra-short pulsed radar

Ultra-short pulsed radar (USPR) reflectometry becomes a variation of the above mentioned technique. Recent developments in microwave components made it possible to reduce pulse width to several picoseconds. It means that the USPRR in principle can reduce the complexity of the pulsed radars considerably by replacing several microwave sources. The ultrafast pulse (1-50 psec) wavepacket consists of wide Fourier spectrum that is enough to cover the major part of density profile (each frequency reflects the corresponding density in the plasma). By separating them in the receiving channel one can obtain the time delay for the sufficient number of frequencies. Those experiments were recently started at GAMMA 10 tandem mirror [57].

2.3.5 Noise radar

Noise correlation radar is a relatively new approach to refectometry systems [58, 59]. A broadband noise signal around a chosen central microwave frequency is transmitted to the plasma and detected after reflection. A fraction of the original signal is fed into an adjustable delay line, which is tuned such that its delay matches that of the plasma path. This is done by determining the correlation

between the plasma and the reference signal as a function of the delay in the reference path. The correlation function is an oscillating signal. The position at which the envelope of the correlation function has a maximum corresponds to the position of the refecting layer.

2.4 Basic principles of pulsed radars

2.4.1 Introduction

Pulsed radar reflectometry was proposed simultaneously in 1990 by two different groups (RTP at FOM, Nieuwegein and TRINITI, Troitsk) in the framework of the diagnostic work for the ITER CDA phase. In pulsed radar reflectometry [54] short microwave pulses (with duration of 1 ns) are launched into the plasma. The basic quantity that is measured is the flight time of the microwave pulses towards the critical density layer and back. In order to obtain the full electron density profile, pulses at many different carrier frequencies have to be launched into the plasma, either simultaneously or successively. Because of its short duration, the pulse has a frequency spectrum with a finite bandwidth $f \pm \delta f/2$ (usually with a Gaussian distribution, if the pulse itself is Gaussian). δf is equal to the inverse of the pulse width.

2.4.2 Advantages and drawbacks of pulsed radars

The advantages of the pulsed radar will be described in the Section 2.4.3. Nevertheless, if fluctuations with short spatial scale lengths are present in the plasma,

the reflected pulse will be like the pulse reflected from a mirror with small-scaled structures frozen into it. Therefore, occasionally destructive interferences may occur and the amplitude of the reflected pulse may become too small to be detected. Since even for very turbulent plasmas a certain number of reflected pulses will still have a high enough amplitude to be detected, it is possible to measure the density profile, albeit at the cost of a decreased temporal resolution. As far as the repetition rate of the pulses is high enough, many data points can be used to compute one time delay with sufficient accuracy. Strong signal losses are mainly observed if one tries to probe the central part of the density profile in low density discharges. In these cases the noise caused by the large quantity of suprathermal electrons in the plasma can prohibit any sensitive measurements to be done with the pulsed radar system [26]. When the pulsed radar refectometer is used to probe the density profile at $r = a > 0.25$, which is usually the case, signal losses are small, even for very turbulent plasmas.

Project background

The presented work here is the first attempt to implement the pulsed radar reflectometry for the helical system. At the present time pulsed radar reflectometry was adopted only for tokamaks and mirror devices.

PULSED RADAR SYSTEMS PRESENTLY INSTALLED IN OTHERS DEVICES

1. **4-channel pulsed radar reflectometer for the RTP tokamak** [3]

[3] FOM-Institute for Plasma Physics, Rijnhuizen, Nieuwegein, Netherlands

- it has been used to diagnose steady state density profiles;
- as well as to follow strong density variations, it detects magnetohydrodynamic instabilities, disruption and pellet injection;

`system is presently moved to the TEXTOR tokamak`

2. **Multifrequency pulsed radar reflectometer for the START tokamak** [4]

   - at present it was operated as a monitoring tool of a density profile evolution

   `first results`

3. **Ultrashort pulse reflectometer for the GAMMA 10 tandem mirror** [5]

   - system is now under development

2.4.3 Comparison with other diagnostics

There are several other diagnostic to obtain the information about electron plasma density. The brief comparison of the diagnostics which are relevant to the plasma density measurements is shown in Table 2.1.

[4] UKAEA Fusion, Abingdon, UK

[5] Plasma Research Center, University of Tsukuba, Tsukuba, Japan

2.5 Short pulse propagation in plasmas

2.5.1 General remarks

In the conventional reflectometry a nearly monochromatic wave is launched into the plasma. Another situation occurs in pulsed radar reflectometry where systems utilize the signals with much larger frequency bandwidth. One has to decompose short pulses into the frequency spectrum for calculation of plasma-pulse interaction. For each frequency the phase delay due to the plasma (see Eq. 2.8) must be found. After this the reflected signal has to be restored by using inverse Fourier transform.

2.5.2 Basics of the broadband pulse propagation

The electric field of the short microwave pulses transmitted to the plasma $u_{trm}(t)$ could be presented as a superposition of the Gaussian-shaped amplitude modulation function [6] and an oscillating signal of frequency ω_0,[7]

$$u_{trm}(t) = \frac{1}{\sqrt{2\pi}\sigma} \exp\left(-\frac{t^2}{2\sigma^2}\right) e^{-i\omega_0 t} \tag{2.18}$$

where $1/\sqrt{2\pi}\sigma$ is the normalizing factor of the Gaussian function. The travel of the pulse through the plasma could be presented as independent propagation of the set of CW oscillations. Mathematically it could be represented as Fourier

[6] in reality this amplitude modulation could be done by driver pulse of the fast microwave switch/amplitude modulator

[7] the quasi-sine continued wave oscillation (CW) of the microwave source (klystrons, BWOs, IMPATT diodes, Gunn-oscillators...)

decomposition of the short pulse,

$$S_{trm}(\omega) = \int_{-\infty}^{\infty} u_{trm}(t)\, e^{-i\omega_0 t} dt \tag{2.19}$$

The power spectrum of the short pulse that has Gaussian shape has to be Gaussian-shaped also,

$$S_{trm}(\omega) = \exp\left(-\frac{\sigma^2(\omega-\omega_0)^2}{2}\right) \tag{2.20}$$

After the reflection from the plasma each frequency from the power spectrum of the launching pulse $u_{trm}(t)$ obtained the additional phase shift $\varphi_{pl}(\omega)$, given by Eq.2.8:

$$S_{ref}(\omega) = S_{trm}(\omega) \times e^{-i\varphi_{pl}(\omega)} \tag{2.21}$$

and reflected pulse $u_{ref}(t)$ could be reconstructed by the inverse Fourier transform from its spectrum:

$$u_{ref}(t) = \frac{1}{2\pi}\int_{-\infty}^{\infty} \exp\left(-\frac{\sigma^2(\omega-\omega_0)^2}{2}\right) \times e^{-i\varphi_{pl}(\omega)} \times e^{i\omega_0 t} d\omega \tag{2.22}$$

We designed pulsed radar reflectometer for CHS with the pulse spectrum that is much smaller than the probing frequency. So, it is unnecessary to evaluate Eq. 2.8 for all frequencies. One can substitute the phase expression to its Taylor-expansion around the probing frequency ω_0:

$$\varphi_{pl}(\omega) = \sum_{n=0}^{\infty} \frac{1}{n!}(\omega-\omega_0)^n \varphi_{pl}^n(\omega_0) \tag{2.23}$$

where $\varphi_{pl}^n(\omega_0)$ the n-th derivative of $\varphi_{pl}(\omega_0)$ with respect to ω calculated around ω_0. For the reliable description of the phase let us use first three terms in its Taylor-expansion. Here we only present final expressions for those terms.

$$\varphi_{pl}^{(0)}(\omega) = \varphi_{pl}(\omega_0) \tag{2.24}$$

The zeroth-order term gives a phase shift for the carrier frequency. It is measured in the case of the conventional fixed-frequency reflectometry.

$$\varphi_{pl}^{(1)}(\omega) = \frac{\partial \varphi_{pl}(\omega_0)}{\partial \omega_0}(\omega - \omega_0) = \tau_{pl}(\omega_0)(\omega - \omega_0) = A \cdot \omega + B \tag{2.25}$$

The first-order term (linear in frequency) gives a phase shift which corresponds to the time delay as given in Eq.2.26:

$$\tau_{pe}(\omega_0) = \left(\frac{\delta\varphi(\omega)}{\delta\omega}\right)_{\omega=\omega_0} = \frac{2}{c}\int_{r_{ant}}^{r_c(\omega_0)} \frac{1}{\sqrt{1 - \frac{\omega_{pe}^2}{\omega^2}}}\, dr \tag{2.26}$$

After reflection from the plasma critical density layer the shape of the microwave pulse remains Gaussian. Due to the plasma dispersion the pulse becomes more broad.

$$\Theta_{ref}^2(\omega) = \Theta_{trm}^2(\omega)\left(1 + \frac{8\ln 2\varphi''(\omega_0)}{\Theta_{trm}^2(\omega)}\right)^2 \tag{2.27}$$

This is the second-order term of the phase. It is quadratic in frequency and represents the effect of the pulse broadening. The expression $\Theta_{trm}(\omega)$ is defined as 'full width half maximum' (FWHM) of the launching pulse:

$$\Theta_{trm}(\omega) = \left(\sqrt{8\ln 2}\right)\sigma_{trm} \tag{2.28}$$

The third-order term represents the asymmetry in the reflected pulse shape.

$$\varphi'''(\omega_0) = \frac{6}{c}\int_{r_{ant}}^{r_{coff}} \frac{\omega_{pe}^2/\omega_0^4}{\left(1 - \omega_{pe}^2/\omega_0^2\right)^{5/2}}\, dr \tag{2.29}$$

To predict the values all these terms were calculated for typical operational parameters of CHS. All calculations were done at fixed frequency $f_0 = 51GHz$, with O-mode polarization, for parabolic density profile with scanned central density

in the range from that just equal to the 'critical density' to that which has the value higher by 100 times . The results of these calculations are shown in Figure 2.4. It is well seen that only for plasma radius where density equals to 97.5% the

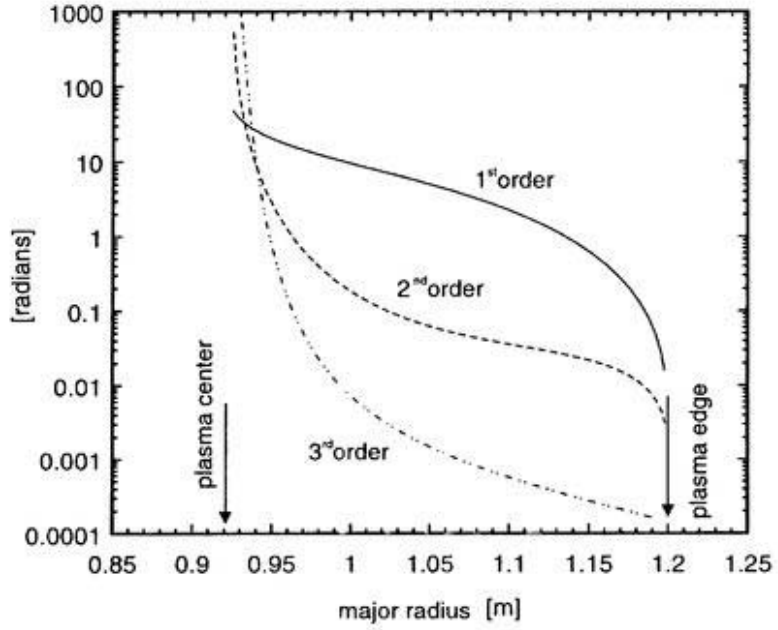

Figure 2.4: *The first three terms in Taylor expansion for the phase of the reflected wave for the CHS plasma with parabolic density profile*

third-order term is equal for the second-order one. So for this and smaller radii the pulse width is not governed by Eq.2.27. However, here WKB-approximation also fails. For the same plasma parameters the time delay and reflected pulse width as a function of CHS plasma minor radius are plotted in Figure 2.5. For the quick calculation of the pulse width and time delay in the one-dimensional

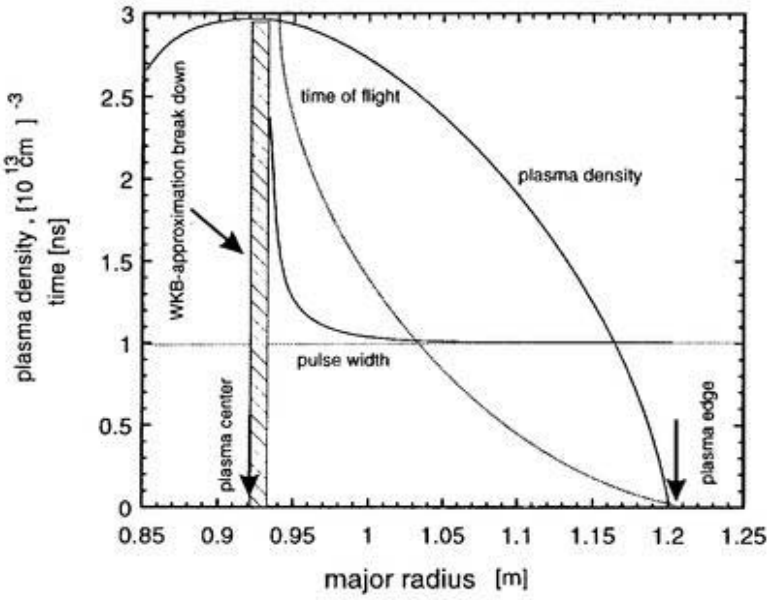

Figure 2.5: *Time of flight and pulse width of the reflected pulse for a transmitted pulse with the width of 1 ns launched into CHS plasma with a parabolic density profile*

approximation it is enough to calculate those values from Eqs.2.26,2.27 and it is not necessary to perform full calculations with Fourier transform.

As it was shown previously significant breakthrough in decreasing the computational efforts was done by replacing FFT calculation of the reflected pulse width and delay time by Eqs.2.26,2.27. But an integral in Eq.2.26 has to be evaluated. However, for some class of plasma density profiles,

$$n_e(r) = n_e(0)\left(1 - \left(\frac{r}{a}\right)^{\alpha}\right)^{\beta} \tag{2.30}$$

it is possible to get analytical solution for this integral. This method was invented by Dr. Pavol Pavlo [60]. We have no intentions to discuss this approach here. Only for reference calculations as for the accuracy we present those formulas here:

$$\tau_{pe}(\omega_0) = \frac{a}{c}\ln\left(\frac{1+X_0}{1-X_0}\right), \quad (\alpha = 2) \tag{2.31}$$

$$\tau_{pe}(\omega_0) = \frac{4a}{c}X_0^2, \quad (\alpha = 1) \tag{2.32}$$

$$\tau_{pe}(\omega_0) = \frac{8a}{c}X_0^2\left(1 - \frac{2}{3}X_0^2\right), \quad (\alpha = 0.5) \tag{2.33}$$

where, $X_0 = \omega_0/\omega_{pe}(0)$.

2.5.3 Accuracy of time of flight approximations

Let us compare the results obtained through the so-called 'full calculation'[8] with those obtained by evaluation in Eqs.2.26, 2.27. The results of such comparison are presented in Figure 2.6. Both calculations were made for the 51 GHz O-mode pulse with the width $\Theta_{trm}(\omega)$=1.0 nsec. The performed calculations show

[8]...calculations of the reflected pulse delay and its pulse width using the Fourier-transform technique are given in Eq.2.22

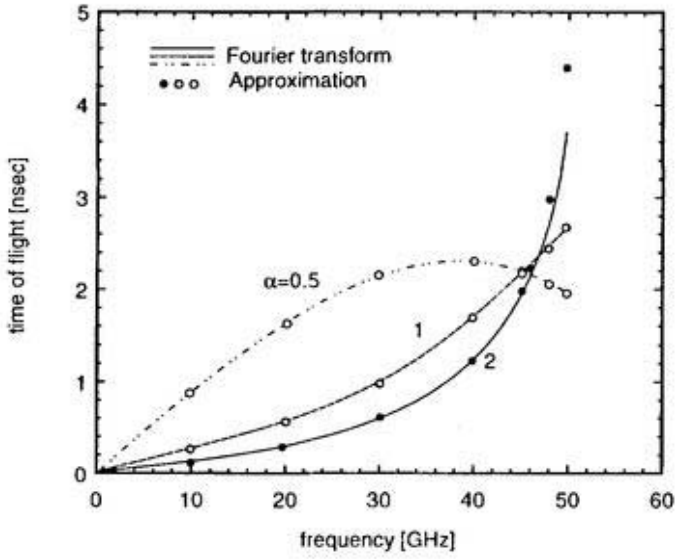

Figure 2.6: *Comparison of the time of flight for Fourier transform calculations and analytical solutions from Eqs.2.31, 2.32,2.33, calculated for CHS plasma with parabolic, linear and square root density profiles.*

that there is a fine coincidence between both approaches, except for highest frequencies in parabolic density profile. For the higher frequencies (f≥50.3 GHz), where $\omega_0/\omega_{pe}(0) \geq 0.93$ WKB-approximation is not valid. Although compari-

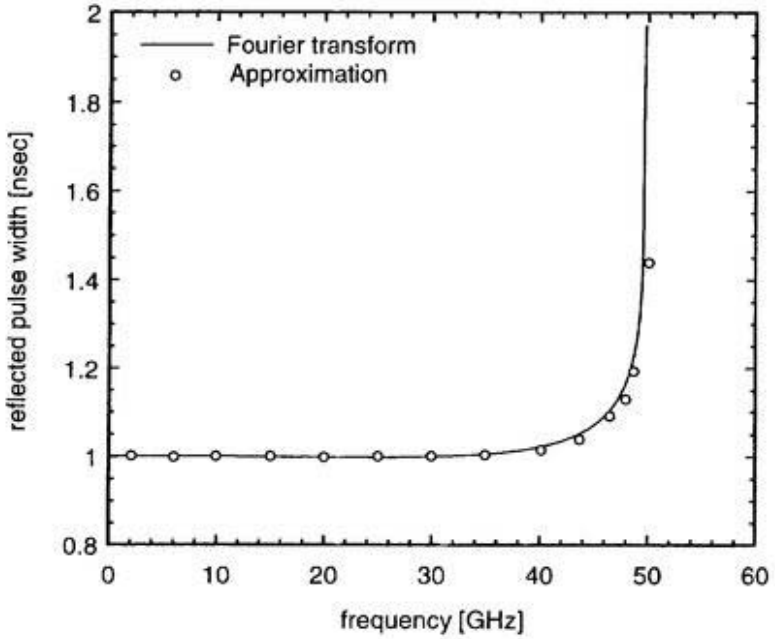

Figure 2.7: *Comparison of change in the pulse width for Fourier transform calculations and analytical solutions for the case of Eq.2.33, calculated for CHS plasma with parabolic density profile*

son calculations for pulse broadening were done. (The results are presented in 2.7). Differencies between both calculations are completely negligible up to the $\omega_0/\omega_{pe}(0) \leq 0.93$. For the more central part of the profile (more high frecuencies) WKB-approximation is not valid.

Diagnostic	Spatial resolution	Time resolution	Advantages	Drawbacks
Interferometry	⊗	⊗⊗	easy to build (standard components)	big plasma access, with two separate ports
FM reflectometry	⊗⊗	⊗	can measure the major part of the density profile;	flat or nonmonolithic profiles; false reflection in transmission lines
AM reflectometry	⊗⊗	⊗⊗	easy to build (standard components)	flat or nonmonolithic profiles; false reflection in transmission lines
Pulsed radars	⊗⊗	⊗⊗⊗	direct measurements; small plasma access	flat or nonmonolithic profiles; several data points; a lot of technical problems
Thomson scattering	⊗⊗⊗	⊗⊗	multipoint diagnostic	difficult to calibrate

Table 2.1: *Main advantages and drawbacks of the electron density diagnostics*

Chapter 3

CHS pulsed radar reflectometer

Pulsed radar reflectometry has been widely developed for plasma density measurements in tokamak plasmas. This work will introduce a first trial to implement this diagnostic for the helical systems. In this chapter we will provide the full description of the CHS pulsed radar reflectometer. An overview of the system components will be followed with the free space propagation measurements. Some specific points of the pulsed radar for the helical systems will be emphasized.

3.1 General introduction

Much attention to the pulsed radar reflectometry and its recent progress were shown by the plasma fusion diagnostics community. Recent experiments, that were carried out at RTP, T-11, START tokamaks, show that pulsed radars could become the promising diagnostic for plasma density profile measurements. The

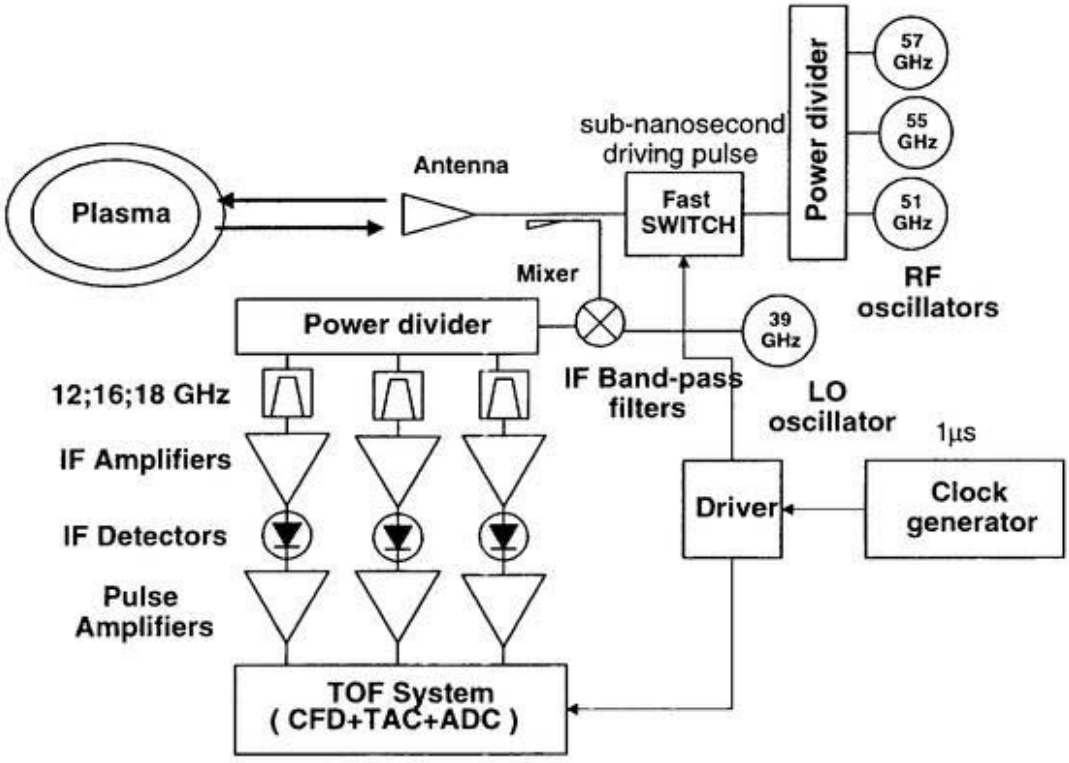

Figure 3.1: *The designed pulsed radar reflectometer for the CHS experiments*

pulsed radar reflectometer, that was designed for CHS experiments, is a one channel (with changeable frequency) system operating in a U-band (40-60 GHz). The

continuous wave oscillation from the transmitters is modulated by fast 'driver' pulse, which is produced by fast pin-switch. Short microwave pulses (with the width of about 1 ns [1]) are launched into the plasma. The time delay between the launched and received (after reflection from the corresponding critical density layer) pulses is measured with a high accuracy. The receiver is of the heterodyne type. It has high dynamic range and large frequency bandwidth. The system is placed 2 m away from the CHS device inside the lead shielding against X-rays. The transmission line mostly consists of Ka band components. To perform the measurements for ordinary and extra-ordinary mode the antenna of the conical horn type is used.

3.2 Transmitter. Driving pulse optimization

The probing signal of continuous wave oscillation is generated by Gunn-type oscillators with the output power of 95 mW for 51 GHz[2] and 80 mW for 55 GHz[3]. At the output of both oscillators an isolation unit is inserted. This prevents the oscillators from the backward radiation. The short microwave pulse is formed by Millitech[4] pin-switch. For producing the short pulse the pin-switch in the Transmission State is being biased with +6.5 V. During isolation state -1.65 V is applied to the pin-switch. As an alternative approach the ultra-fast IRE varactor-

[1] actually the Full Width Half Maximum

[2] Millitech Voltage-Controlled Gunn Oscillator CDV-19 series

[3] MDT (Microwave Device Technology Corporation) MGM55 series

[4] Millitech High Speed PIN Switch PSH-19 series

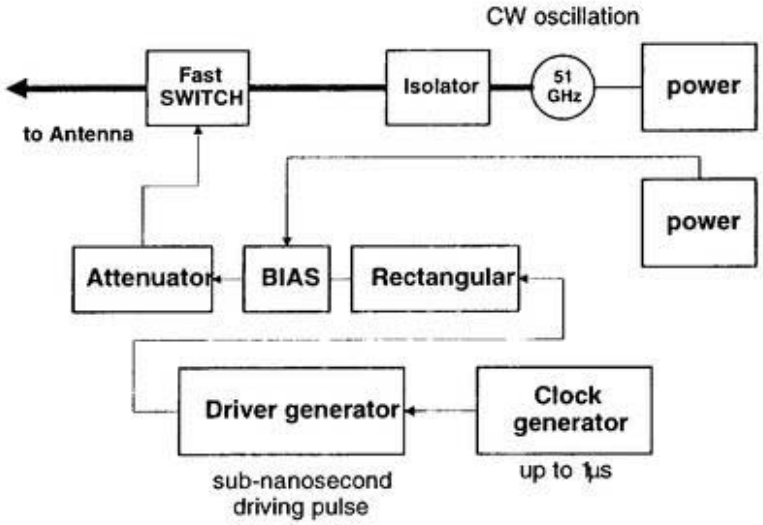

Figure 3.2: *The scheme of the pulsed radar transmission system*

diode modulator[5] was used for the CHS experiments. The main advantage of this modulator is to have extremely small pulse width. We could achieve the value of 210 ps with the same isolation/insertion loss characteristics. The weak point of this device is its narrow band (55±0.25 GHz), compared with Millitech PIN switch (54±3 GHz). As the driver for fast switches the PicoSecond Labs 2000D series generator has been used. The output amplitude is 45 V. In the case of Millitech the rise and fall times of the driver pulse were 0.65 and 1.06 ns (FWHM=1.05 ns) respectively. To decrease the rise and fall times of the driver, the 300 ps, -6 dB rectangular-network unit was inserted. This allowed decreasing the driver pulse width down to 800 ps. To get an appropriate input amplitude at

[5]designed and assembled by the group of Dr.G.Ermak in Institute of Radiophysics and Electronics of the Ukraine, Ak.Proscura st. 12, Kharkov, Ukraine

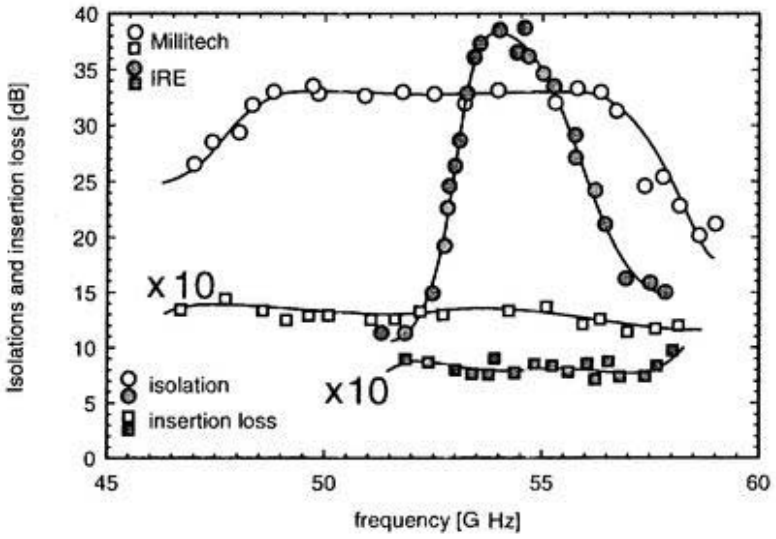

Figure 3.3: *The measured isolation and insertion loss of the pin-switches for U-band*

the pin-switch and to avoid the backward reflection to the driver -6dB additional attenuator was inserted. The insertion point was chosen in the front of PIN-switch. After the modulation of the PIN-switch the 75 mV pulse of 1.02 ns or 0.21 ns (for Millitech or IRE switches respectively) width is launched through the transmission line into the plasma. Because the ON/OFF ratio depends on the frequency the isolation and insertion losses of the pin-switches in the U-band were measured. The results are plotted in Figure 3.3.

Two microwave pulses produced by both switches (Millitech and IRE) are also presented in Figure 3.4.

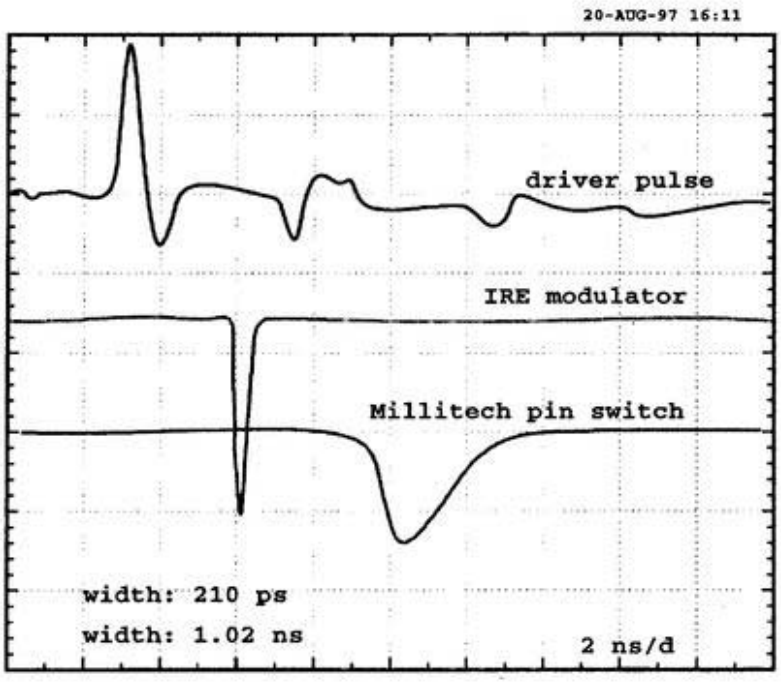

Figure 3.4: *The comparison of the output microwave pulse shape between Millitech and IRE switches/modulators*

3.3 Transmission line and antenna system

At the beginning we tried to place the system outside the lead wall. For this we installed a set of X-band ($22.86 \times 10.16\ mm^2$) and Ka-band ($7.112 \times 3.556\ mm^2$) waveguides. The total length of the WG system was 8.8 m. The total attenuation in the waveguide system has to be found from calculation and from direct test measurements. The theoretical attenuation in a rectangular copper air-filled waveguide operating in TE_{10} mode is given by [61] :

$$\alpha = \frac{1.47 \times 10^{-4}}{a^{1.5}} \times \frac{\frac{a}{2b}\left(\frac{f}{f_c}\right)^{1.5} + \left(\frac{f}{f_c}\right)^{-0.5}}{\sqrt{\left(\frac{f}{f_c}\right)^2 - 1}}\ dB \cdot m^{-1} \tag{3.1}$$

It was found that there are a strong backward multiple 'false' reflections from the WG corners, tapers, etc. These reflections decreased the performance of the system. Therefore it was decided to withdraw the WG system and to put the pulsed radar more close to CHS.

As an antenna we used standard 20 dB gain conical horn antenna. This allows us to use both polarization modes as the injected wave. To increase the gain of the antenna the Teflon lens was tested and installed. This gives us a possibility to increase the outgoing power to the plasma by 15%, and to increase the reflection from plasma by 24%.

3.4 Vacuum break issues

For vacuum break the thin 0.5 μm MICA window was installed. It was assembled in the special flange. Because waveguides of a circular cross section must be at-

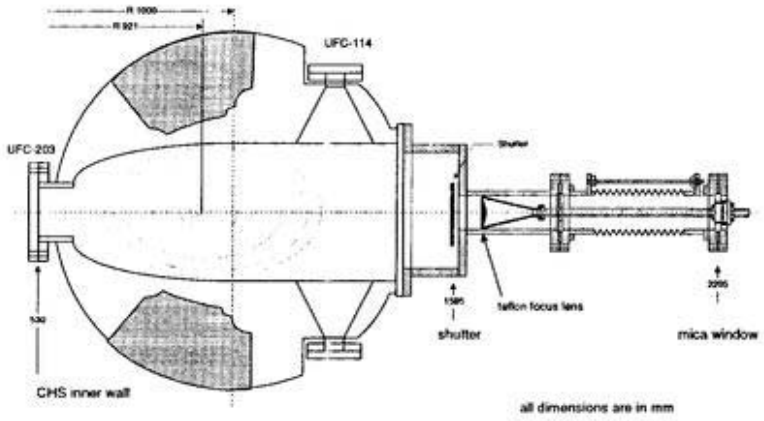

Figure 3.5: *The diagnostic port for the CHS pulsed radar reflectometer*

tached to the antenna, special rotation waveguide unit was inserted. It is possible to gradually change the incoming wave polarization. It is very useful because of significant shear of CHS [6]. The measurements of the reflectivity coefficient (it is shown in Figure 3.6) were done to get a value of the power reflected backward.

3.5 ECH band rejection filter

In the CHS experiments the main plasma production method is with ECH. The ECH system operates at the frequency of 53.2 GHz and could significantly deteriorate pulse radar measurements. To protect receiving system from high ECH power the band rejection filter is used. This filter has a sharp peak of the attenuation at the frequency of 53.2 GHz. The theoretical and measured characteristics of the filter are shown in Figure 3.7. The measured insertion losses are plotted

[6] see Table 1.1 in the Chapter 1

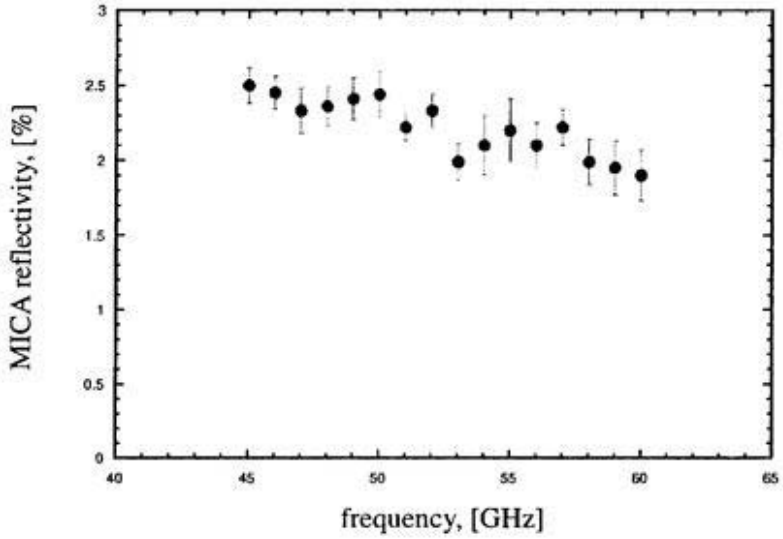

Figure 3.6: *The reflectivity of the MICA vacuum break window in U-band frequency range*

in the same figure and they show the attenuation of the receiving signal due to filter insertion. It seems that this insertion loss has not a significant influence on the SNR or the reflected microwave pulses.

3.6 Detection by a balanced mixer

Because of the complicated three-dimensional structure of the plasma in CHS much higher attenuation of the reflected signal is expected. For getting of the suitable SNR of the reflected pulses heterodyne techniques are applied. This yields higher dynamic range than when the direct microwave detection is used. The local oscillator (LO) that drives mixer consists of Gunn oscillator of 39 GHz. The IF frequency is 12 and 16 GHz for 51 GHz and 55 GHz RF oscillators,

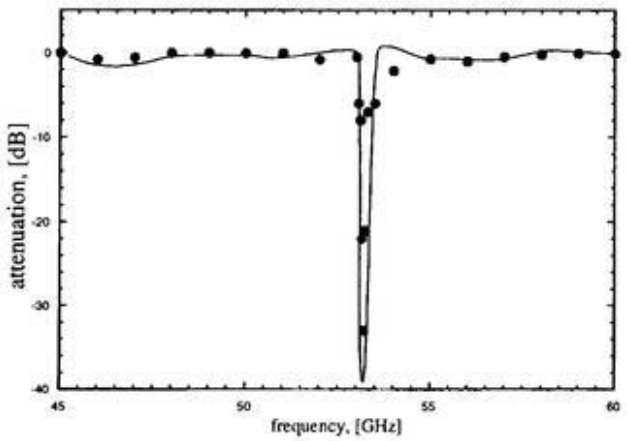

Figure 3.7: *The theoretical and measured characteristics of the band-reject filter*

respectively. The power output from LO is set to be 13dBm that allows to achieve the best performance level of the mixer. The conversion loss of the mixer is -4dB.

After the reflection from the plasma a short pulse travels backward through the antenna system. At the -3dB directional coupler one half of the reflected power comes to the balanced mixer input. Before detection, IF signal from the mixer is filtered with 12 or 16 GHz band pass filter and amplified with IF amplifier with the gain of 23dB. After that the signal was detected by Spaceck A302 fast response video detector. To get a sufficient pulse amplitude for driving the time of flight measurements system we use an additional video amplifiers with total gain of 22dB.

It must be noted that for the first preliminary measurements we used a single RF detection technique instead of balanced mixer. The SNR for this type

of detection was 240 times smaller than that of heterodyne one. This difference is presented in Figure 3.8.

Because of placing the detection part of the reflectometer close to CHS the problem of the non-disturbed pulse transmission occurs[7]. To overcome the significant pulse broadening the special types of cables[8] are used.

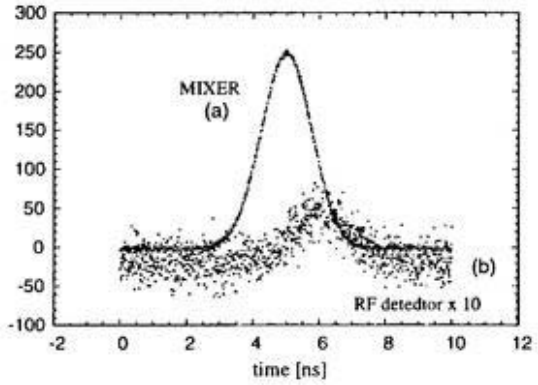

Figure 3.8: *The detection of the reflected pulse by using balanced mixer (a) and RF detector (b).*

3.7 Free space propagation tests

Before installing the pulsed radar in CHS it was tested at the laboratory. The plasma reflection was simulated by the aluminum plate that was placed in front

[7] to transmit the pulses from the detection part to the electronics without shape changes

[8] semi-rigid 50 Ohm coaxical cables

of the antenna at the distance of about 1 m. The position of the reflecting plate could be changed with the precision of 1mm. To perform the test under

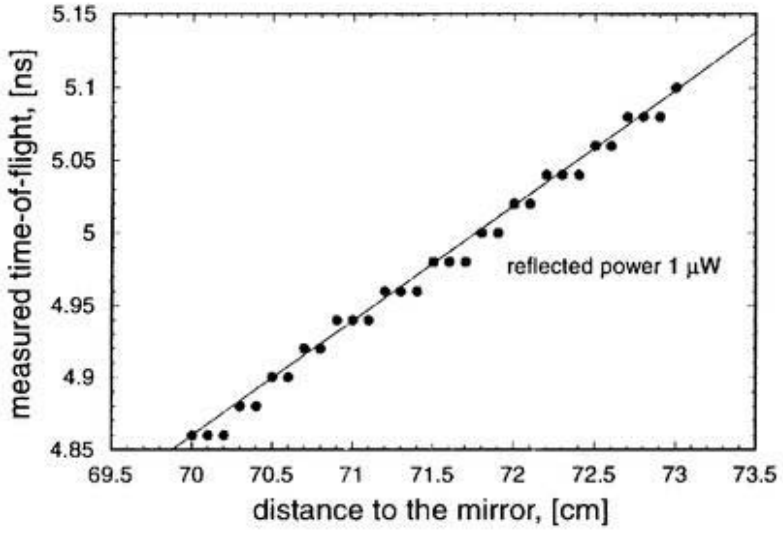

Figure 3.9: *The free space propagation test of the pulsed radar*

the condition, much more close to CHS plasma experiments, the vacuum break unit was also inserted in waveguide system. To simulate large pulse amplitude modulations, that could happen in the plasma, the transmitted power from the RF oscillators is varied from 25 to 1 % (approximately to 1 mW). The experiments show the good agreement of the measured values with theoretical time of flight in the free space. It is seen that measured time of flight values look like multi-step function. One can easily obtain the errors in the reflector position from this step length. Those errors are from 2 to 4 mm. So, during this free space propagation test it was found that the position of the reflector could be measured within the accuracy of 3 mm.

3.8 Timing pick-off technique

The criteria for spatial resolution of modern fusion diagnostics could probably be set as 1 cm. This spatial accuracy (in vacuum) means a timing accuracy of 70 ps in the time of flight measurements. To investigate the fast changing plasma phenomena the modern diagnostic must have $1 - 5 \times 10^5$ measurements per second. All sub-nanosecond time measurements are based on the precise time definition of the start-stop event. In the case of the pulsed radar it means the picosecond range precision in determination of the arrival time for pulses reflected from the plasma. For our measurements the Constant Fraction Discrimination (CFD) technique was chosen. This was done because the main advantage of this method is that the timing is the same for the constant shaped pulses with high amplitude changes (insensitivity for amplitude fluctuations due to the attenuation of the reflected pulses by the plasma).

3.8.1 Constant fraction discrimination technique

The measurements , presented in this work, are performed by using of EG&G Ortec Model 9307 pico-Timing discriminator. It defines the arrival time of the analog pulses from ultra-fast detectors with picosecond precision. It accepts the pulses with amplitude ranging from -50mV to -5V, and pulse width from 400 ps to 5 ns FWHM. However, CFD is affected by the pulse shape deformation, which arises from the dispersion of plasma. Another source of errors comes from the plasma density fluctuations and microwave beam refraction.

CFD outputs generate a negative NIM standard pulse. The leading

edge of the outputs precisely marks the time of the arrival of the pulse from the detector (reflected pulse from plasma (or inner wall of the device)). This CFD output through the cables connects to the STOP input of the Time-to-Amplitude Converter (TAC). The reference pulse from the main CLOCK of the timing system has been used as START pulse for the TAC. The TAC measures the time interval between START/STOP pulses and produces the analog output pulse proportional to the measured time, because it is based on the principle of charging the capacitor with a constant current source during the time between START and STOP pulses. The TAC we used in the experiments is EG&G Ortec Model 566. It has an accuracy of about 10 ps and a highest repetition rate of about 400 kHz.

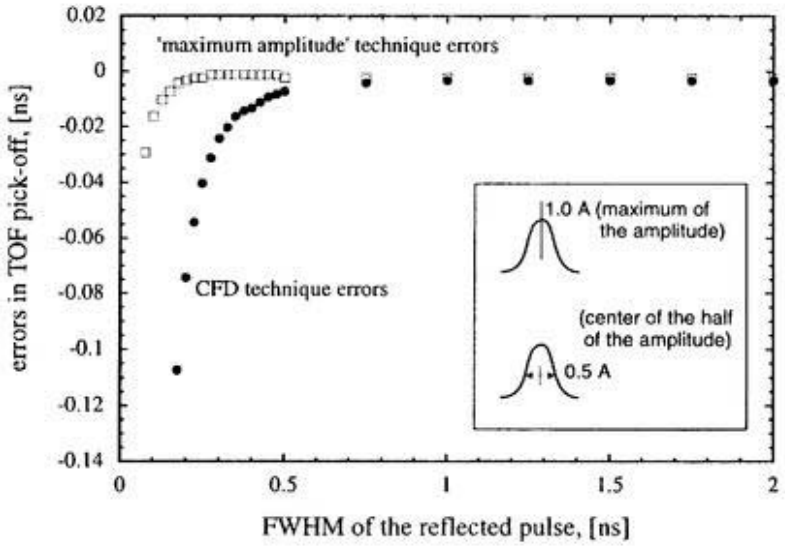

Figure 3.10: *The errors estimation of the CFD and 'maximum' amplitude timing pickoff techniques*

A numerical simulation has been done to estimate the CFD timing errors (see Figure 3.10). From these calculations we can conclude that the pulse deformation is more serious for shorter pulse width, and this deformation leads to a larger errors in the timing. We have found that the errors are negligible for the pulse width longer than 0.5ns for a specific CHS case. The accuracy of the pulsed radar timing comes from the SNR of the reflecting signal. Noise due to the plasma or electronics gives the additional, sometimes significant errors. The time accuracy could be represented by:

$$\Delta t = \frac{\Theta_{ref}(\omega)}{\ln 2\sqrt{2SNR}}, \tag{3.2}$$

where $\Theta_{ref}(\omega)$ is FWHM of the reflected pulse. For the case of 1 ns microwave pulse to achieve the spatial resolution (in vacuum) of 1 cm[9] the time accuracy should be as follows:

$$\Delta t = 2.3183 \times 10^{-4} \cdot \Theta_{ref}(\omega), \tag{3.3}$$

which implies that the SNR must be at least 232 or 23.65 dB. This value is less that the measured one during detection technique comparison test ($SNR_{test} \approx 240$).

[9]...this spatial resolution corresponds to 67 ps in the timing accuracy ...

Chapter 4

Experimental results

In this chapter we present the main experimental results from the pulsed radar reflectometry. An experimental investigation into electron plasma density measurements via pulsed radar reflectometer with *monostatic antenna arrangement* has been done for the first time in *helical systems*. Those experiments have been performed for different regimes of the CHS operation. Measurements with a good temporal and spatial resolution coincide with those from Thomson scattering and interferometer data. In the case of X-mode measurements the calculated radial profile of the magnetic field is used. By means of the pulsed radar fast density changes during pellet injection have been observed. Localized MHD oscillations were measured during low-β plasma experiments.

4.1 Reflectometry in CHS

In this section measurements with pulsed radar reflectometer are presented. The measurements were done in two campaigns. At first the measurements were done without time of flight (TOF) measurement system. This situation was originated from existence of the false reflection from the vacuum break MICA window. The amplitude of those reflected pulses was higher than or the same order as those from the plasma. During second campaign the dual-switching technique was implemented (this will be discussed in section 4.1.2) that allowed the successful run of TOF system. Also the measurements in low density discharges are presented. This is so-called 'delayometry' regime of operation for pulsed radar.

4.1.1 Measurements of the time delay of the microwave pulses

Because of the extremely strong attenuation of the reflected pulse from the CHS plasma, (due to unfavorably complicated (3-dimensional) plasma shape in the helical system[1]) the amplitude of the reflected signal was much smaller than the amplitude of the pulses that were reflected from the vacuum break MICA window. This fact does not allow the use of timing electronic because the reflection from the window occurs earlier than the reflection from the plasma in the interested

[1]... the previously reported experiments, that were carried out in several tokamaks, did not have those problems, because of quasi-cylindrical plasma configuration. In the above mentioned experiments the amplitude of the false pulses reflected from the vacuum break was smaller, that allowed direct use of time pickoff systems from the very beginning.

time domain. That is why, at the first stage of experiments for timing measure-

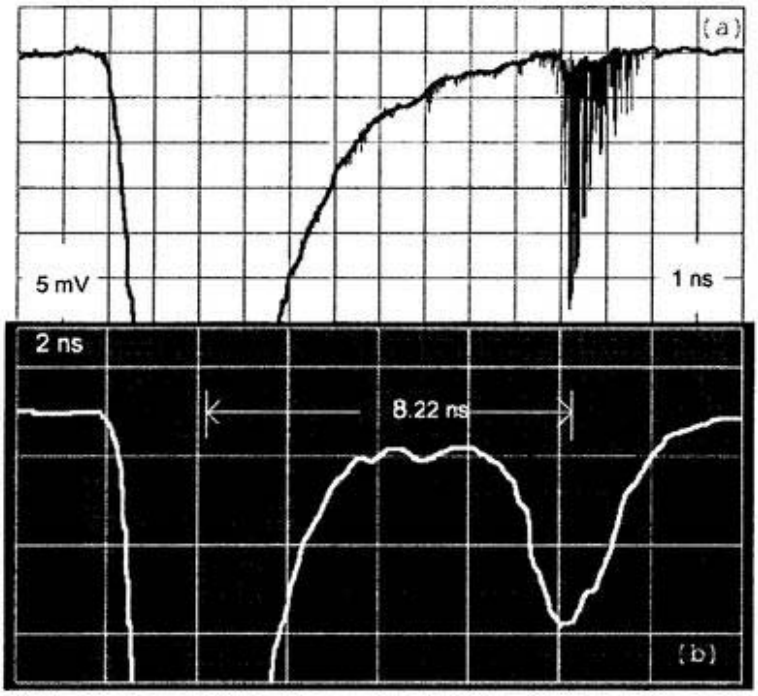

Figure 4.1: *The envelopes of the reflected pulse from the vacuum break window and from the plasma obtained with sampling (a) and digital (b) oscilloscopes*

ments, the detection via fast oscilloscopes has been used. In our experiments we tried sampling [2] and fast digital[3] oscilloscopes. Because of characteristic of sampling oscilloscope, it requires about 10,000 pulses (10 ms) to make a reflected pulse waveform. When the amplitude modulation is very large, each point, which corresponds to a single pulse measurement, scatters and the resultant waveform

[2]Yokogawa DL 8100 series sampling oscilloscope, with the bandwidth of 10 GHz

[3]ultrafast LeCroy 9362 digital oscilloscope with the bandwidth of 0.75 GHz

becomes noisy (Figure 4.1(a)). This scatter makes us to measure the time delay accuratelly. The error came from the scatter of each point in the waveform, and they are much larger than those obtained at a free space propagation test with a flat mirror and with time measurement electronics (TAC).

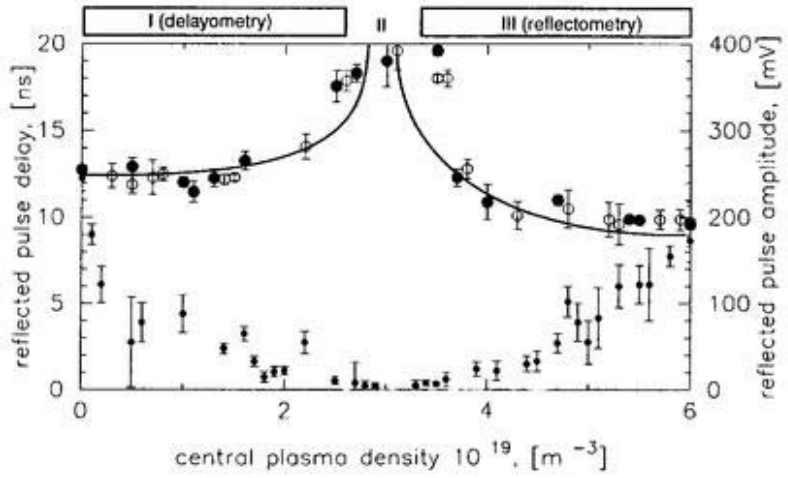

Figure 4.2: *Reflected pulse delay (open circles - IBW+NBI plasma, solid circles - ECH+NBI plasma), calculated pulse delay for parabolic density profile (solid line) and reflected pulse amplitude (diamonds) as a function of the central electron density for ordinary mode case.*

The measurements of the time delay in CHS plasma were done for both polarization modes. The plasmas were initiated by IBW (Ion Bernstein Wave) or ECH and heated by NBI and ECH. These measurements were done for discharges with the magnetic field of 0.85 T and maximum electron density of about $6 \times 10^{19} m^{-3}$. To obtain the dependence of the time of flight (delay of pulses) on the

plasma for different central density we changed the 'observation window' (with the time duration of 10 ms) for the shots when plasma conditions are fixed. Without plasma the reflected pulses are stable and the measurement is accurate. The small difference between the measurement and calculation is probably due to unsmooth surface of the inner wall (there is port with the figure-8 like shutter at the inner side of the vacuum chamber), so it is difficult to define the accurate distance to the inner wall.

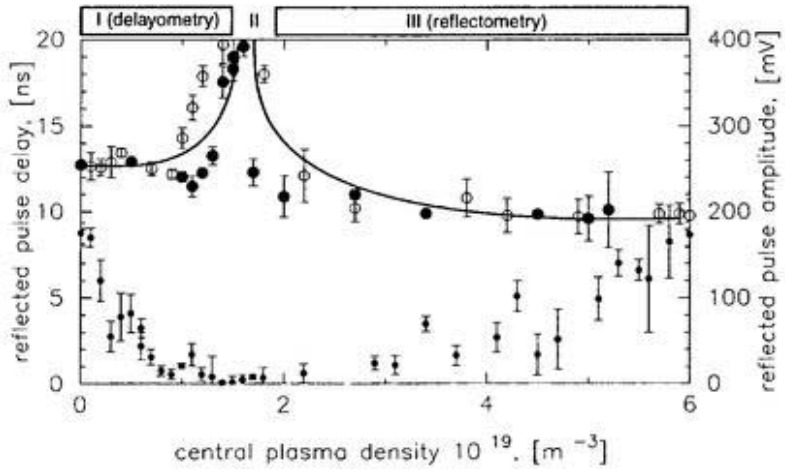

Figure 4.3: *Reflected pulse delays (open circles - ECH+NBI plasma, solid circles - ECH+NBI plasma), calculated pulse delay for parabolic density profile (solid line) and reflected pulse amplitude (diamonds) as a function of the central electron density for extraordinary mode case.*

Figures 4.2, and 4.3 show the time delay and amplitude of the reflected pulses as a function of the central electron density. The measured data can be di-

vided into three regions. The region I is the low density one, where the CDL does not exist in the plasma and launched wave passes through the plasma. In this case the system is operated as an interferometer. The amplitude of the reflected pulses decreases with the density. This is probably due to the refraction of the microwaves in low-density plasma. The region III is the high density one, where the CDL exists and the amplitude increases as the CDL moves towards the antenna. In the region II adjacent to appearance of reflecting layer the reflected pulses are not observed (possibly due to the strong refraction of microwaves). Figures 4.2 and 4.3 also show calculated time delay for both modes. The density is estimated from the data of line density obtained by an HCN laser interferometer [6], by assuming a parabolic density profile. The measured data on reflected pulse delay follow the calculated curves, but error bars are rather large. This comes from the strong amplitude modulation of the reflected pulse during measurements[4]. As shown by the measurements and calculations, the densities where reflected pulses begin to appear are different for O/X modes. To change the microwave polarization an additional 90 degree twisted waveguide section must be inserted. This was the main reason of the mismatch of the time delay at the 'zero' density (at the begining of the discharge).

[4]...let us remind that those pulse delay measurements were averaged (due to the measurements with the sampling oscilloscope) in a 10 ms time window...

4.1.2 Dual-switching technique. Canceling of false reflection.

There are several possibilities to diminish an influence of false reflection from the MICA window. First, it is by increasing the effective reflected power from the plasma. This could be done by tuning the antenna alignment. But this operation is very restricted because of small diagnostic port which is utilized for the pulsed radar. From the same point of view the installation of the double-antenna system is not allowed, too. The only thing we could do in this situation was the replacement of the antenna with the lens loaded one. This antenna combines conical horn (with diameter of 45.72 mm and length of 83.82 mm) and plano-convex Teflon lens. This antenna offers a high gain, narrow beamwidth with Gaussian beam shapes and low sidelobes. Another significant improvement

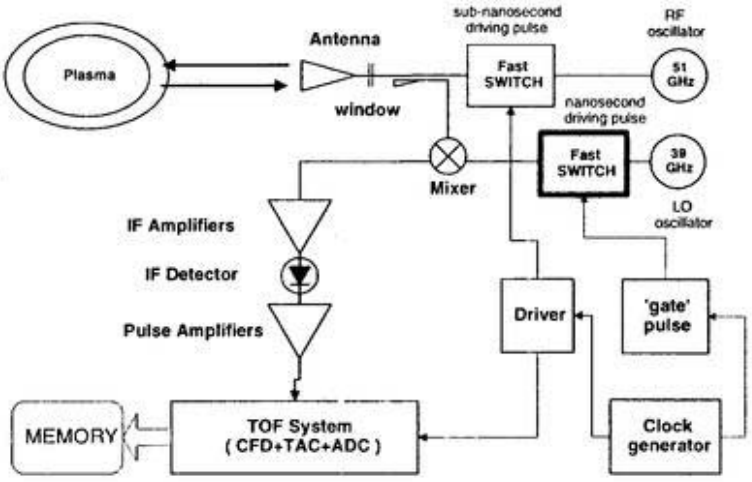

Figure 4.4: *The double-switching (gated receiver) pulsed radar reflectometer*

is to change pulsed radar setup to the dual-switching scheme. Those scheme is shown in Figure 4.4. The idea of this improvement lies on the additional 'time-gating' of the reflected signals. As was shown, two reflected pulses come from single launched one. One is reflected from the vacuum window and arrives earlier than that reflected from the plasma. The second 'gating' switch is inserted in front of the mixer. It is allowed to be opened only for times corresponding to the reflection from the plasma and from CHS inner wall. That is why the 'false'

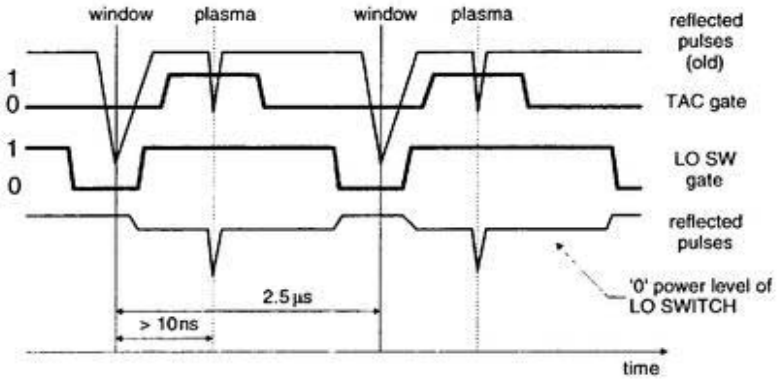

Figure 4.5: *Schematic waveforms of the gated receiver*

pulse from the window does not come to the mixer and is not accepted by the electronics[5].

[5]...it must be noted that previously we tried the same kind of gating at the electronic stage, but because of long ON/OFF transaction time of the TAC gate function $\geq$ 5ns, it was impossible to implement it; another possibility to suppress reflection from the window is to construct the 'additional' reflected pulse with the same timing but opposite polarity...

4.1.3 Plasma density measurements

O-mode experiments The CHS pulsed radar performance is presented at first by an overview of its response to the various plasma discharges, and secondly by comparison of the obtained data (after 'time to density inversion') from pulsed radar with the density profiles measured with Thomson scattering and far-infrared interferometry [11, 12].

As it becomes clear from probing frequencies range of pulsed radar, a high density plasma is needed for the successful operation as a reflectometer. In the case where the polarization of the microwaves has been chosen as ordinary, for 51 GHz operation, the density of $3.22 \times 10^{19} m^{-3}$ is required. High density regimes were obtained in plasma with ECH production and NBI (co. inj) heating, sometimes with additional ECH heating. Measurements were done for the discharge that is presented in Figure 4.6. The time evolution of pulsed radar reflectometer and the time behavior of the line averaged density obtained by means of HCN laser interferometer is shown. From the beginning of the discharge, during first several milliseconds, there is no plasma and clear reflection from the inner wall of the device is observed. The time of flight completely matches the theoretical one of the pulse propagation in a free space. From 11-12 ms of the discharge the heating systems begin to produce plasma, but the density in those time period is rather low and is below the critical density for pulsed radar reflectometer. As the group velocity in the plasma is smaller than in vacuum, the time of flight increases compared with the vacuum situation. Pulsed radar reflectometer operates like interferometer[6]. The 53.2 GHz ECH radiation disturbs the radar signal

[6]...this is so-called delayometry regime, which will be discussed below...

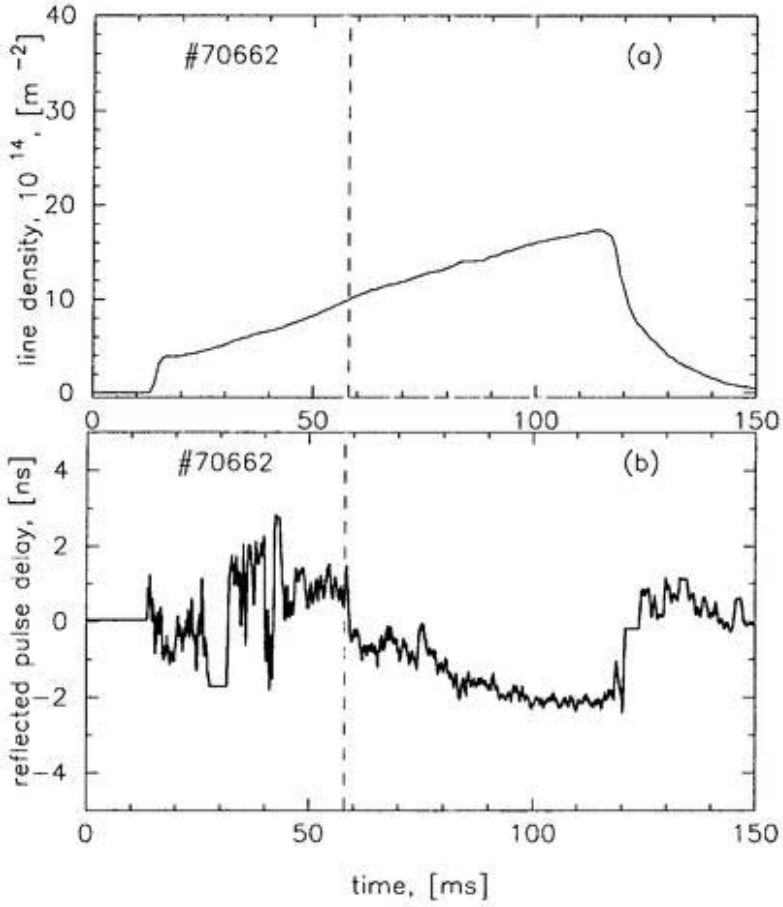

Figure 4.6: *Temporal evolutions of line averaged plasma density(a) and time of flight of the short microwave pulse (O-mode) measured by pulsed radar reflectometer for 51 GHz (O-mode polarization) (b) for the discharge 70662. The vertical lines indicate the timing when a reflecting layers appear in the plasma (from the interferometry data). The time of flight in vacuum to the inner wall is defined to be zero.*

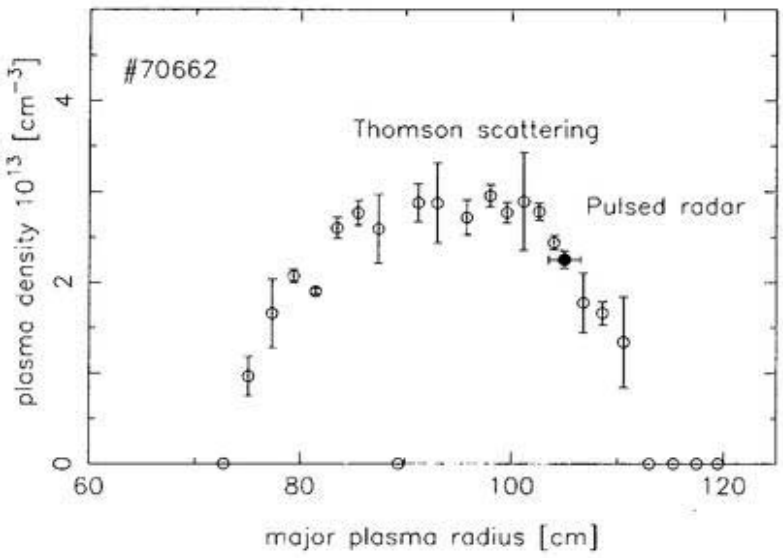

Figure 4.7: *Comparison of pulsed radar data with density profile from Thomson scattering for the discharge 70662, presented in Figure 4.6*

significantly. After some time the density exceeds the critical one and a fast sudden decrease in flight time occurs. From this moment pulses launched into the plasma are reflected from the corresponding critical density layer and additional point (per one frequency) can be calculated from pulsed radar measurements.

An inversion of the measured time of flight to density values was made by Abel-inversion routine, with the assumption of the plasma boundary position from the Thomson measurements. The profile plotted for the time 90 ms is shown in Figure 4.7. Rather good agreement between the plasma density measured with the pulsed radar and that from Thomson scattering, is observed. Note that for those measurements the maximum central density in the discharge was higher by only 15% than the critical density for the frequency of 51 GHz. And the reflection at that time occured at the central part of the plasma.

It was decided to change polarization to the X-mode for the next campaign. This allows the reflection of the pulses from comparatively low plasma density. The alignment of the polarization was chosen in such a way, that the wave has quasi-pure X-mode orientation at the edge of the CHS plasma.

X-mode profile reconstruction It is impossible to reconstruct plasma density profile from the single-channel pulsed radar data only. This is because of utilizing one launching frequency in present configuration. Nevertheless, it is possible to estimate the spatial position of the reflecting point in the plasma. If the magnetic field profile is known and plasma density profile could be already determined (from any other diagnostic, i. g. multichannel interferometry, Thomson scattering or O-mode reflectometry) then the position of reflection layer is

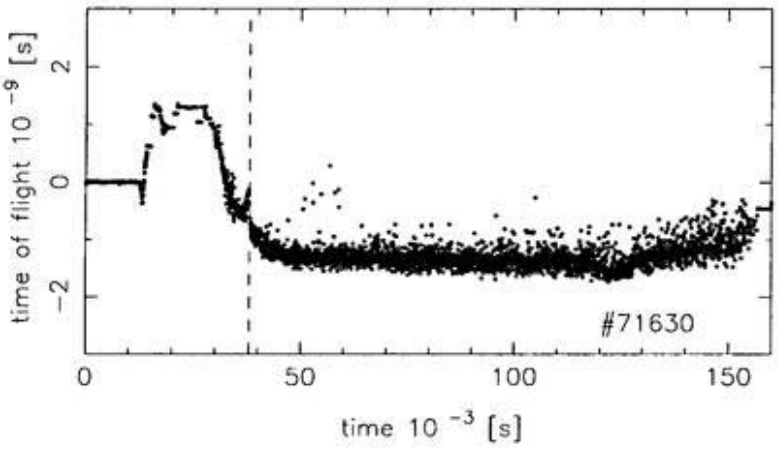

Figure 4.8: *Temporal evolutions of time of flight of the short microwave pulse measured by pulsed radar reflectometer for X-mode polarization, for the discharge 71630*

possible to derive.

In the case of CHS experiments for time-to-distance conversion plasma density profile obtained from the Thomson scattering data. For the densities below the cut-off one, 'virtual time delay' is calculated for the assumed profile (linear and parabolic functions have been used for the profile fitting[7]). The Abel transform procedure could not be applied (becouse of structure of the dielectric function) but must be derived from recurence formula instead:

$$x_n \approx x_{n-1} + \frac{1}{4}\tau(\omega_n)v^{gr}(\omega_n, x_i) - \sum_{i=0}^{n-2}\left\{\frac{1}{v^{gr}(\omega_n, x_i)} + \frac{1}{v^{gr}(\omega_n, x_{i+1})}\right\}(x_{i+1} - x_i) \tag{4.1}$$

where v^{gr} is group velocity and x_i is the position of i-th cutoff layer correspond-

[7]The initial parameters of the plasma density profile have been varied to check the influence the edge gradient on the time-of-flight.

ing to the frequency ω_i. The reconstruction is starts from plasma edge, where we can assume $v^{gr} = c$. The comparison between plasma density obtained from the pulsed radar measurements and Thomson scattering profile reconstruction is presented in Figure 4.8. Those experiments were carried out for IBW plasma production. Without ECH radiation the scattering of the radar data becomes much smaller, that comes from the better reflection conditions due to the favorable plasma density (two times higher than the critical density) for those experiments. It was found from timing error (scattering of the data) that the temporal

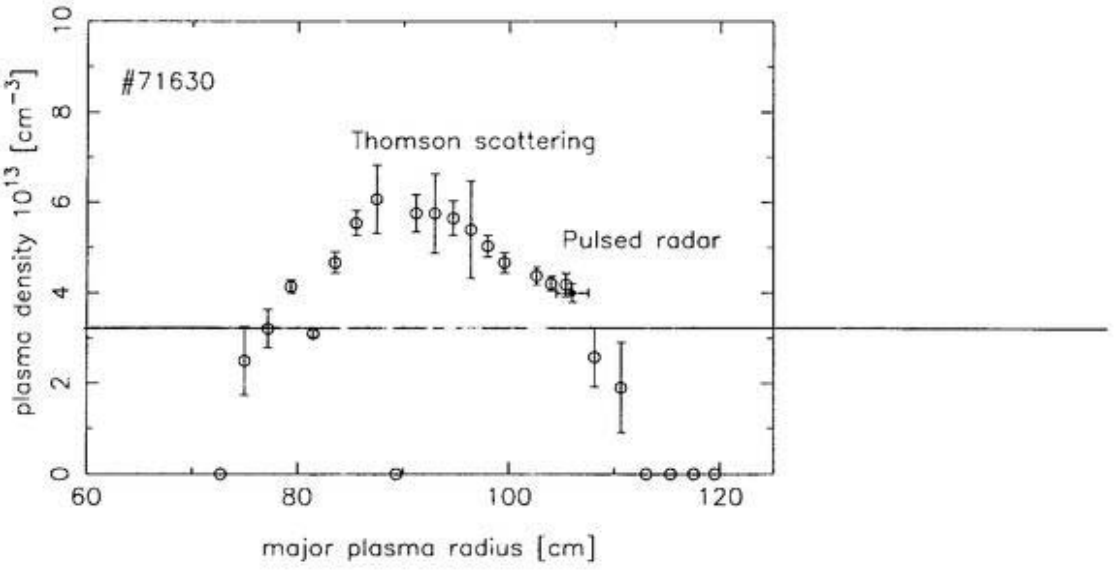

Figure 4.9: *The comparison of pulsed radar data with density profile from Thomson scattering, for the discharge 71630*

resolution of 100 ps was achieved. This corresponds to the spatial resolution of 1.25 cm in free space.

4.2 Ice pellet injection experiments in CHS

High repetition rate of the pulsed radar reflectometer measurements makes it possible to follow the rapid changes of plasma density after the pellet injection in the CHS plasma. In Figure 4.10 the time evolution of the main plasma parameters during such kind of experiments is presented. The hydrogen ice pellet with the diameter of about 1 mm is injected into NBI plasma with low density. HCN laser interferometer could not follow fast changes of density and gave unphysical data. Here we will discuss those experiments. For several shots, which depend on pellet dimensions, pulsed radar reflectometer successfully measures time of flight during these fast phenomena (rapid changes in the plasma density). The changes in the time delay mean that the cut-off density layer moves rapidly to the edge of the plasma. It is seen that larger pellets caused bigger additional fueling of the plasma density, but it seems that the 'penetration' length is keep constant. By those experiments it was shown that the pulsed radar can follow high-speed density transition in the plasma even when the interferometer does not work.

4.3 Delayometry in CHS

In the regimes with the maximum density above the cut-off density, a pulsed radar relies on the total reflection of the electromagnetic waves by the plasma. The time neccessary for transmitted narrow pulse to complete a round trip to the critical layer in the plasma and back to the antenna is directly measured and

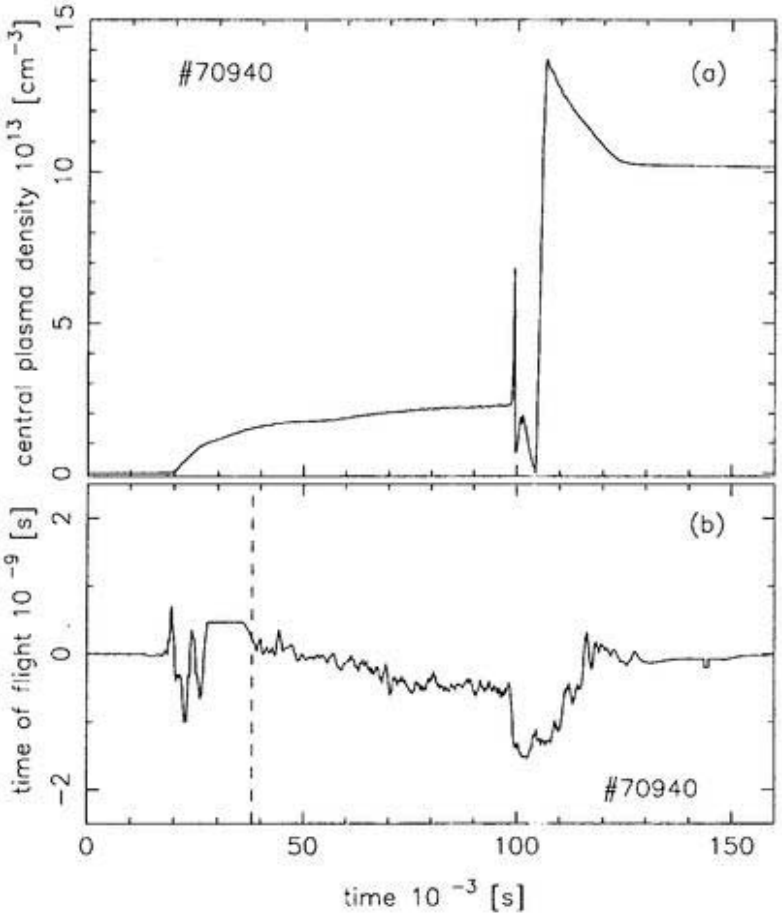

Figure 4.10: *Temporal evolutions of central plasma density (a) and time of flight of the short microwave pulse measured by pulsed radar reflectometer for X-mode polarization (b) for the discharge 70940 during ice pellet experiments.*

is given by a formula:

$$\tau_p(\omega) = \frac{\partial\varphi(\omega)}{\partial\omega}|_{\omega=\omega_0} = \frac{2}{c}\int_{r_c}^{a}\frac{dr}{\mu(\omega)} \tag{4.2}$$

In low density plasmas, where the maximum density is below the critical density corresponding to the probing frequency, pulses launched into the plasma will not be reflected but pass through the plasma. They will be reflected by the inner wall of vacuum vessel, returned and detected. As the group velocity v_g of the pulses in the plasma is lower than that in vacuum $v_g = \frac{\partial}{\partial k}(\mu(\omega)\cdot\omega)$, an increase in the time of flight with respect to the vacuum situation is detected. The incremental pulse delay (for O-mode) is given by:

$$\tau_p(\omega)^* = \frac{2}{c}\int_{-a}^{a}\left(\frac{1}{\mu(\omega)} - 1\right)dr \tag{4.3}$$

In both formulas (for both equations Eq. (4.2), Eq. (4.3) and v_g) $\mu(\omega)$ means plasma refractive index for O-mode pulses, and could be written from the `Appleton-Hartree` formula [8]:

$$\mu(\omega) = \sqrt{1 - \frac{\omega_{pe}^2(r)}{\omega_0^2}} \tag{4.4}$$

in Eq. (4.2) the factor two is originated from the double pass through the plasma. If we expand Eq. (4.3) around the probing frequency ω_0 we can obtain:

$$\tau_p(\omega) = \frac{2}{c}\int_{-a}^{a}\sum_{n=1}^{\infty}\frac{(2n)!}{2^{2n}(n!)^2}\left(\frac{\omega_{pe}^2(r)}{\omega_0^2}\right)^n dr\ , \tag{4.5}$$

The first term in the sum is proportional to the average plasma density.

$$\overline{n_e} = \frac{1}{a}\int_0^a n_e(r)\,dr \tag{4.6}$$

[8] only in the cold plasma approximation, e.g. the phase velocity $v_{ph} = \mu(\omega)\cdot\omega/k$ of the wave is close to the vacuum speed of light, and the motion of the ions can be neglected

The remaining terms can be neglected. Equations (4.2) and (4.5) represent functionally independent branches of $\tau(\omega)$ which is discontinuous at $\omega = \omega_p(max)$. So, we can rewrite the average density expression in terms of the incremental time of flight in such a way:

$$\overline{n_e} \cong \frac{c\tau_{pe} n_{cr}}{2a} , \tag{4.7}$$

where n_{cr} is the cut-off density of the corresponding cut-off frequency. Using the value for the CHS plasma diameter (53.5 cm) and a relation criteria between launching frequency $f_0 = 54.9\ GHz$ [9] and plasma critical density:

$$n_e^{crit} \equiv n_{cr} = 1.24 \times 10^{-4} f_0^2 \ , [\times 10^{14} cm^{-3}] \ , \ [f_0 \text{ in GHz}] \tag{4.8}$$

equation Eq. (4.7) yields:

$$\overline{n_e} = 1.04 \times 10^{13} \tau_{pe} \ , \quad [\tau_{pe} \text{ in ns}] \tag{4.9}$$

The limitation of applicability of this formula comes from the fact that the second term in Eq. (4.5) must be less than 10 percent of the first term. It means that the line-average density in the CHS discharges must be below $0.4 \times 10^{13}\ cm^{-3}$. For the densities that become closer to cut-off it is necessary to include more higher term in Eq. (4.5). For wide range of profiles it is possible to calculate the increase in the time of flight analytically. For parabolic profile the increased (with respect to vacuum) time of flight is:

$$\tau(\omega_0) = \tau_0 \left(\frac{\omega_0}{2\omega_{pe}(0)} \ln \left(\frac{\omega_0 + \omega_{pe}(0)}{\omega_0 - \omega_{pe}(0)} \right) - 1 \right) , \tag{4.10}$$

where $\omega_{pe}(0)$ - central plasma frequency, $\tau_0 = 4a/c$ - vacuum time of flight.

[9] $f_0 = 2\pi\omega_0$

As an example of delayometry operation the low density discharge is depicted in Figure 4.11. For the time that does not overlap with ECH pulse the agreement is rather good.

4.4 Observation of the MHD activity in CHS plasmas

Another area, where pulsed radar could be applied, is measurement of the plasma MHD oscillations. The understanding of the nature of these phenomena gives additional information for the configuration optimization , stability and transport properties of the CHS plasma. The observation of the local plasma electron density fluctuation was performed during low-β experiments ($\beta \sim 0.2\%$). Figure 4.12 shows the temporal behaviour of the reflected pulse delay. One can see the clear fluctuations of time delay during 70 - 85 ms. It was found that these fast changes in the time delay strongly correlate with magnetic probe measurements. In Figure 4.13 one can see the expanded view of those traces. These oscillations could be originated from the magnetic islands rotation. As another confirmation of this idea, we present the comparison of the spectra for the magnetic probes and reflectometry data in Figure 4.14.

In this chapter we just introduced some of the possibilities of the pulsed radar as a diagnostic tool for investigation of the various plasma parameters. These experiments had the primary aim to check the performance of PRR operation in the helical systems. It was found that the general behaviour of this diagnostic tool is very close to those that operate on the tokamaks. Among dis-

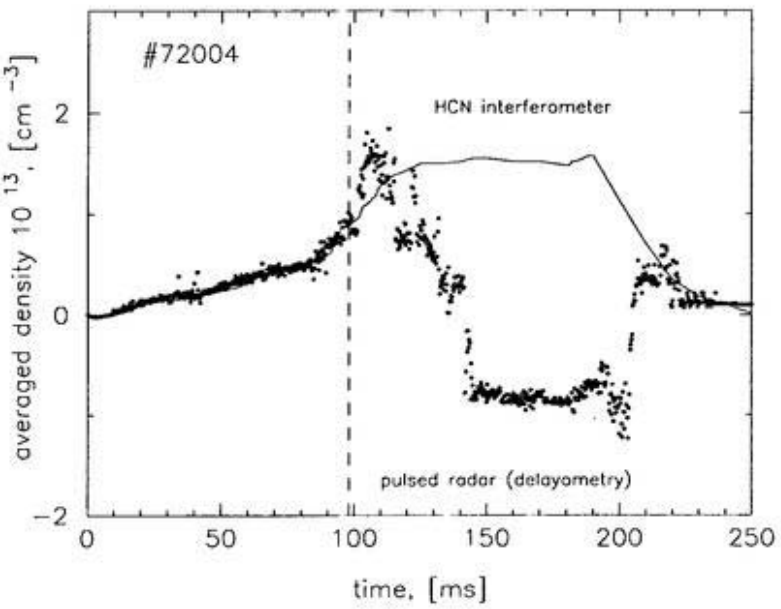

Figure 4.11: *Temporal evolutions of time of flight of the short microwave pulse measured with pulsed radar reflectometer for 51 GHz and line averaged plasma density (solid line) during low density regime (delayometry operation). The vertical line indicate the timing when a reflection becomes more dominant, and delayometry operation transforms into pure radar one; data from the right side of the dashed line ($t > 98ms$) have no physical meaning).*

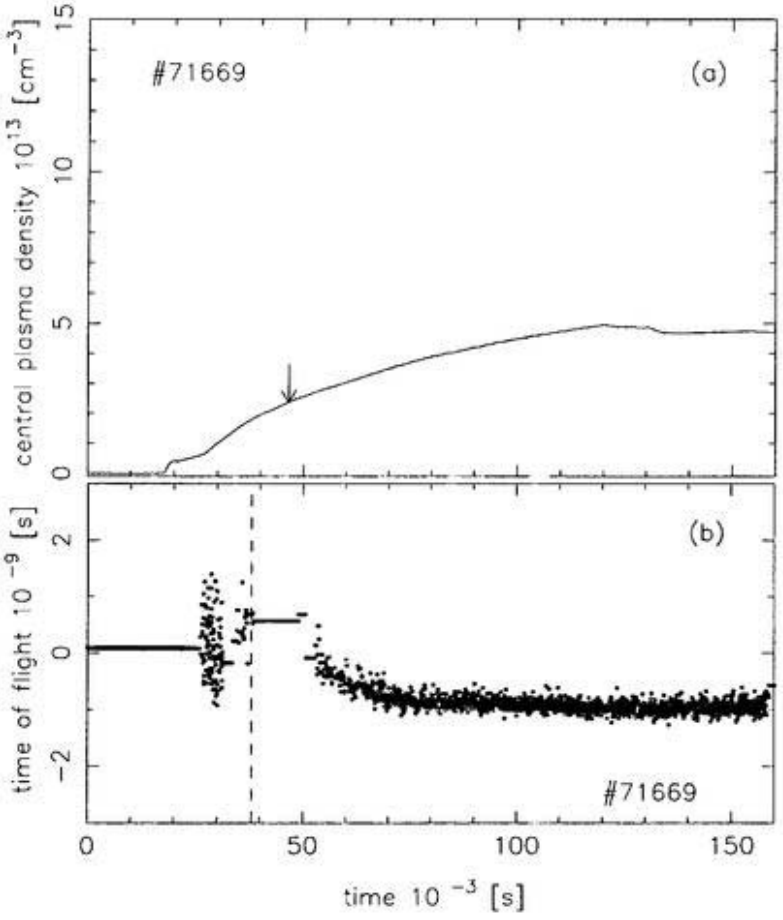

Figure 4.12: *Temporal evolutions of central electron density (a) and time of flight of the short microwave pulse (b) measured with pulsed radar reflectometer during low-β operation.*

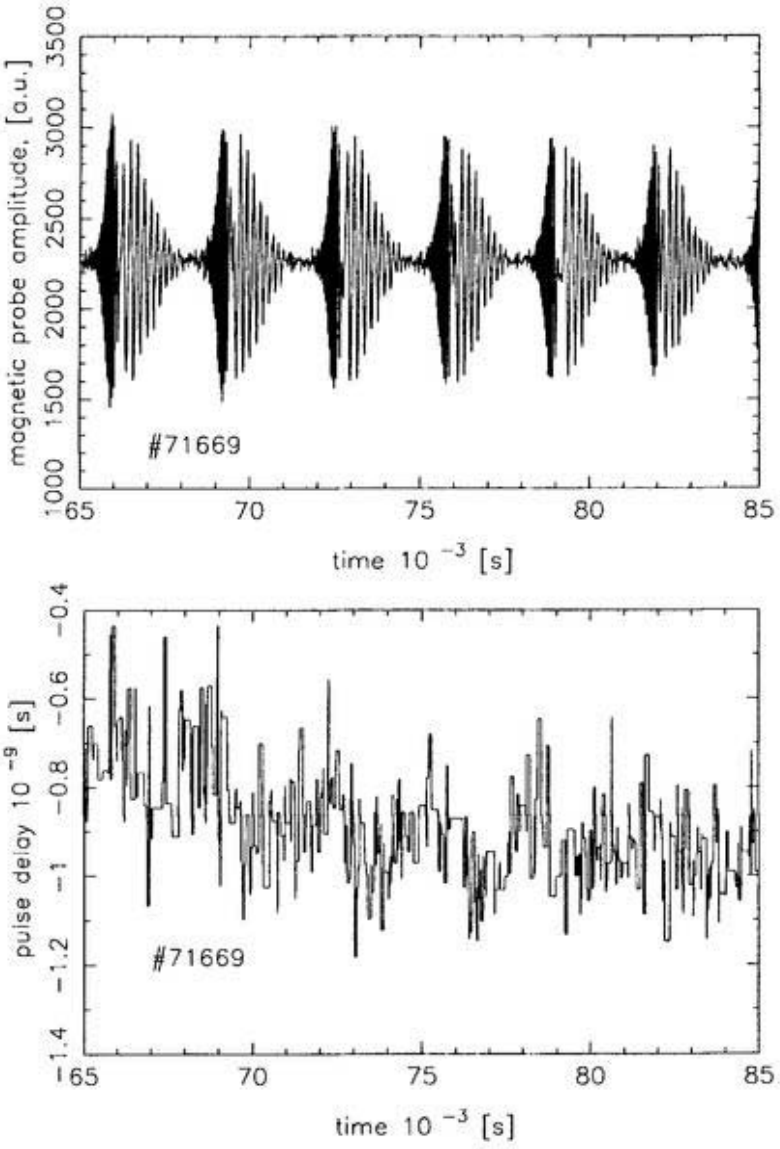

Figure 4.13: *Trace of the magnetic probes (a) and the radar (b) signals during 60-85 ms for the same discharge as shown in Figure 4.12.*

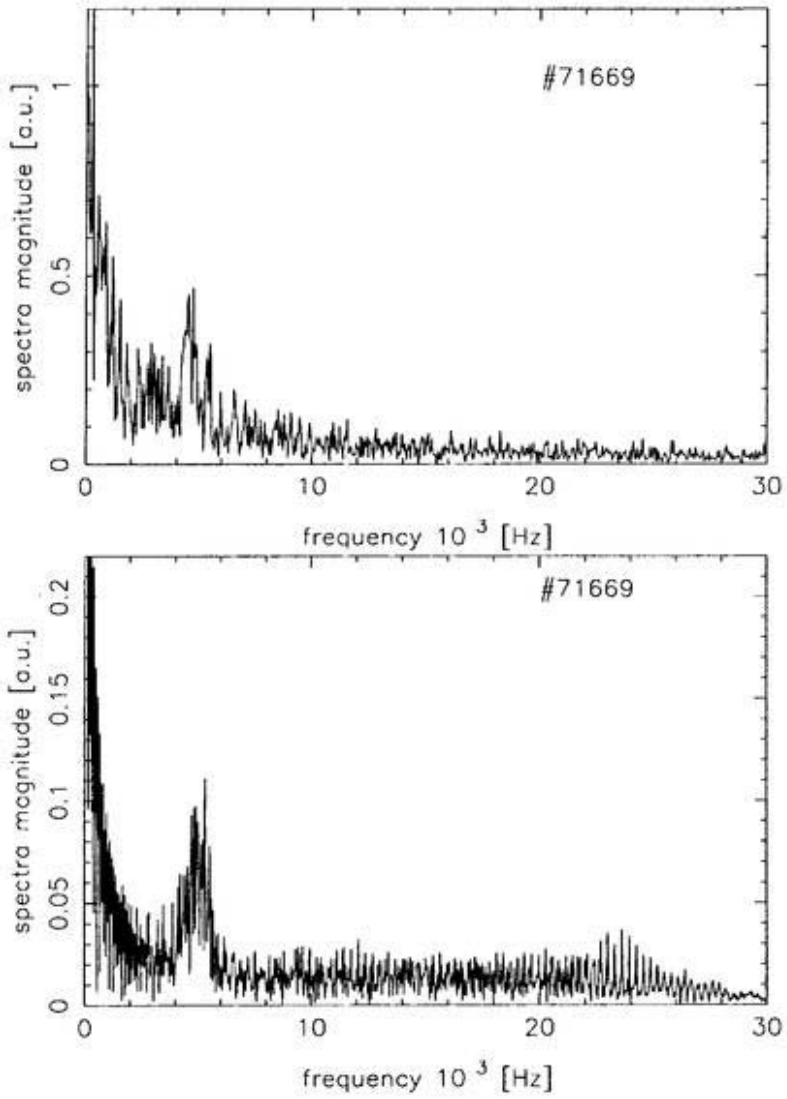

Figure 4.14: *Comparison of the power spectrums of the radar signal (a) during 60-85 ms and of the probes (b) for the same time window; and for the discharge as was shown in Figure 4.13.*

tinctive features for the helical systems that must certainly be mentioned we must point out several items.

- real three-dimentional topology of the reflected surfaces (it means small reflected power and additional problems with antenna arrangement, limited port access);
- non-negligible shear (the deduction of the magnetic field and the effect of mode coupling becomes more difficult);

Chapter 5

Summary

In this thesis we presented results of the first application of the pulsed radar reflectometer for helical confinement system- CHS device. In the process of development of the CHS pulsed radar reflectometer and its use in experiments on CHS we met and solved some problems specific for helical plasmas (diminution of plasma backscattered pulse due to strong plasma reflecting layer curvature) and for CHS radar porting (strong vacuum window reflection in a single launching/receiving antenna scheme).

'False' pulse canceling was done by use of the probing beam focusing and by elimination of window reflection via the dual-switching technique. Single frequency radar can measure the position of only one plasma layer and for the real plasma density profile reconstruction the number of radar channels has to be increased. Nevertheless first experiments with single frequency pulsed radar on CHS showed its benefits in regimes with rapid changes of plasma density (pellet injection experiments). It's worthwhile to mention that the pulsed radar in CHS

is working in the most difficult conditions as compared with other operating pulsed radars: smallest plasma radius, strongest curvature of reflecting plasma layer, single antenna scheme.

All these difficulties will be strongly diminished for pulsed radar operating on larger helical devices. There is no hesitation that the multifrequency pulsed radar reflectometer can be developed and used on LHD for plasma density profile reconstruction with the radial accuracy of 0.005 - 0.01 m. Multifrequency radar can be used also for correlation reflectometry fluctuation studies of the edge plasma in LHD.

Due to high repetition rate of the measurements it becomes possible to evaluate the fast plasma phenomena such as plasma collapse during pellet ablation and middle range (up to 50 MHz) plasma density fluctuations. It was found that during low-β experiments those fluctuations may have magnetic islands rotation as their origin.

During specific CHS regimes with low density (less than $10^{12} cm^{-3}$ it is possible to use pulsed radar as delayometry/interferometry measurements. The data obtained during delayometry experiments perfectly agree with HCN interferometer ones.

Finally we showed the feasibility of the monostatic antenna arrangement (single launching/receiving antenna) approach for ITER pulsed radar reflectometry.

For the new medium-sized l=2 helical devices (CHS-qa) much more attention must be paid for the proper antenna (antennas) alignment. Because those devices aim at the further understanding of plasma matter (not fusion reactor

capability demonstration) two antenna scheme of the pulsed radar reflectometer is preferable. Also much improvement could be done by the installation of the 'special type' antenna which will allow to probe the elliptically shaped plasma along the small axis.

From the technical point of view this work has introduced the construction of the microwave pulse that is two times shorter[1] than that used in previous experiments (moderate pulsed radars only) in other laboratories[2].

[1]... microwave pulse of 210–230 ps was obtained

[2]... here we mean the moderate pulsed radar, not their ultra-short pulsed competitors...

Comments on the pulsed radars for the LHD and CHS-*qa*

The experience of operation of the CHS pulsed radar reflectometer (PRR) allows considering a possibility of application of PRR on other helical devices of NIFS - LHD and CHS-*qa*. Taking into account the set of diagnostics already developed or proposed for these devices the PRR systems for LHD and CHS-*qa* could be used for solution of specific task - determination of edge plasma electron density profiles with high spatial and time resolution. Our experience and state of art of development of PRR components allow to make a suggestion that the spatial resolution of 0.005 - 0.01 m and time resolution of 1 μs are feasible. All advantages of PRR could be used if the multifrequency systems with the number of frequency channels of 10-15 are used. Our experience allows to suggest that the single launch/receive antenna for each channel of PRR could be used with porting of each antenna on special flange placed in equatorial plane of devices. As we have an experience of using one antenna for plasma probing by 2 different frequencies, the special R&D aimed on development of antenna/waveguide systems with larger number of PRR frequency channels (3-5) will be beneficial for

diminishing number of antenna ports. The development of antenna/waveguide systems with enlarged frequency pass-band will be beneficial also for implementation of correlation reflectometry in these devices. This will allow studying edge plasma fluctuations - the very popular and informative theme of toroidal confinement research. Plasma probing by both - O- and X- modes is possible. The same kinds of gated superheterodyne receivers can be used for the reflected signal detection. Larger plasma radius of these new devices will result in a diminution of refraction effects on reflected power (it scales as $\sim r_{pl}^2$). In its turn it will result in more favorable ratio of "plasma-to-window" reflected signals and will diminish problem of suppression of false reflection in single launching/receiving antenna system.

Bibliography

[1] L. Spitzer, Jr., Phys. Fluids, **1** (1958) 258.

[2] A. Iiyoshi *et al.*, Fus.Technol., **17** (1990) 169.

[3] C. Beidler *et al.*, Fus.Technol., **17** (1990) 148.

[4] J. Hofmann *et al.* Plasma Phys. Controlled Fusion, **38** (1996) A193.

[5] C. Jaenicke *et al.*, Plasma Phys. Controlled Fusion, **37** (1995) A163.

[6] H. Maaßberg *et al.*, Proc. 24^{th} EPS Conf., Berchtesgaden, Germany, **17** (1997) Paper No. P.4056.

[7] S. Okamura *et al.*, Nucl. Fusion, **35** (1995) 283.

[8] K. Matsuoka *et al.*, IAEA-CN-50/I-I-I *in Plasma Physics and Controlled Fusion Research*, Proc. 12th IAEA Conf., Nice, France (1988) 411.

[9] K. Nishimura *et al.*, Fus.Technol., **17** (1990) 86.

[10] A. Fujisawa *et al.*, Rev. Sci. Instrum., **67** (1996) 3099.

[11] A. Fujisawa *et al.*, Phys. Plasmas, **4** (1997) 1357.

[12] K. Ida *et al.*, Rev. Sci. Instrum., **60** (1989) 867.

[13] K. Ida *et al.*, Phys. Rev. Lett., **76** (1996) 1268.

[14] S. Okamura *et al.*, Annual Report of NIFS, (1995) 206.

[15] S. Okamura *et al.*, Annual Report of NIFS, (1997) 222.

[16] K.G. Budden, 'Radiowaves in the Ionosphere', *Pergamon Press, Oxford*, (1970).

[17] V.L. Ginzburg, 'The propagation of the electromagnetic waves in plasma', *Pergamon Press, Oxford*, (1970).

[18] A. Costley, Diagnosis of fusion plasma using reflectometry, in *International School of plasmap physics "Piero Caldirola" Proc. of the cource and workshop held in Varenna, Italy*, (1986) 379.

[19] M. Manso *et al.*, Plasma Phys. Controlled Fusion, **35** (1993) B141.

[20] C. Laviron *et al.*, Plasma Phys. Controlled Fusion, **38** (1996) 905.

[21] N. Bretz *et al.*, Nucl. Fusion, **34** (1994) 1283.

[22] J. Sanchez *et al.*, Rev. Sci. Instrum., **64** (1993) 487.

[23] T. Tokuzawa *et al.*, J. Appl. Phys., Part 1, **60** (1995) L76.

[24] A. Silva *et al.*, Rev. Sci. Instrum., **67** (1996) 4138.

[25] A. Hugengoltz *et al.*, Rev. Sci. Instrum., **62** (1991) 1100.

[26] S. Heijnen *et al.*, Rev. Sci. Instrum., **66** (1995) 419.

[27] V. Shevchenko *et al.*, Rev. Sci. Instrum., **68** (1997) 2040.

[28] TFR Group *et al.*, Nucl. Fusion, **18** (1978) 647.

[29] J. Doane *et al.*, Rev. Sci. Instrum., **52** (1981) 12.

[30] F. Simonet *et al.*, Rev. Sci. Instrum., **56** (1985) 664.

[31] H. Bottolier-Curtet and G. Ichtchenko *et al.* Rev. Sci. Instrum., **58** (1987) 539.

[32] A. Hubbard *et al.*, J. Phys. E:Sci. Instrum., **20** (1987) 423.

[33] E. Anabitarte *et al.*, J. Phys. D:Appl. Phys., **20** (1988) 1384.

[34] M. Manso *et al.*, Proc. 16th EPS Conf.on Control. Fusion and Plasma Phys., Volume **13B** (1989) 1517.

[35] T. Fukuda *et al.*, Proc. 4th Internat. Sympos. on Laser-aided Plasma Diagnostic, Volume **2** (1989) 13.

[36] A. Costley *et al.*, Rev. Sci. Instrum., **61** (1990) 2823.

[37] E. Doyle *et al.*, Proc. 17th EPS Conf.on Control. Fusion and Plasma Phys., Volume **14B** (1990) 1596.

[38] G. Hanson *et al.*, Rev. Sci. Instrum., **63** (1992) 4658.

[39] E. de la Luna *et al.*, Rev. Sci. Instrum., **66** (1995) 403.

[40] A. Sips *et al.*, Plasma Phys. Controlled Fusion, **35** (1993) 743.

[41] C. Hugenholtz *et al.*, Rijnhuizen Report, **90-192** (1990).

[42] J. Sanchez *et al.*, Plasma Phys. Rep., **20** (1994) 1.

[43] A. Skibenko *et al.* Plasma Phys. Report, **20** (1993) 7.

[44] M. Moresco *et al.*, Rev. Sci. Instrum., **66** (1995) 406.

[45] P. Buratti *et al.*, Rev. Sci. Instrum., **66** (1995) 409.

[46] T. Tokuzawa *et al.*, Jpn. J. Appl. Phys., **34** (1995) L76.

[47] K. Kim *et al.*, Rev. Sci. Instrum., **66** (1995) 1229.

[48] M. Hirsch *et al.*, Rev. Sci. Instrum., **67** (1996) 1807.

[49] J. Doane, Rev. Sci. Instrum., **51** (1980) 317.

[50] J. Sanchez *et al.*, Rev. Sci. Instrum., **63** (1992) 4654.

[51] C. Domier *et al.*, Rev. Sci. Instrum., **63** (1992) 4666.

[52] C. Domier *et al.*, Rev. Sci. Instrum., **66** (1995) 339.

[53] L. Bruskin *et al.*, Rev. Sci. Instrum., **69** (1998) 425.

[54] T. Estrada *et al.*, Rev. Sci. Instrum., **61** (1990) 3034.

[55] S. Hamberger *et al.*, Phys. Rev.Lett., **37** (1976) 1345.

[56] T. Tokuzawa *et al.*, Rev. Sci. Instrum., **68** (1997) 443.

[57] S. Kubota *et al.*, Jpn. J. Appl. Phys., **37** (1998) L300.

[58] V. Korosteljov, R. Pavlichenko *et al.*, Proc.of the IAEA Technical Comm. Meeting on microwave reflectometry for fusion plasma diagnostics, **Part II** (1992) 236.

[59] K.Lukin, R. Pavlichenko *et al.*, Proc. of International symposium 'Physics and Engineering of millimeter and sum-millimeter waves, **Part III** (1994) 682.

[60] P.Pavlo, Czech. J. Phys., **43** (1993) 51.

[61] T. Moreno, *Dover Publication Inc., New York*, (1948).